LIMNOLOGY and OCEANOGRAPHY



Limnol. Oceanogr. 67, 2022, 1911–1930 © 2022 The Authors. Limnology and Oceanography published by Wiley Periodicals LLC on behalf of Association for the Sciences of Limnology and Oceanography. doi: 10.1002/lno.12175

Transitioning global change experiments on Southern Ocean phytoplankton from lab to field settings: Insights and challenges

Philip W. Boyd ^{1*} Scott C. Doney, ² Sam Eggins, ³ Michael J. Ellwood ³, Marion Fourquez, ^{1,a} Brook L. Nunn, ⁴ Robert Strzepek, ¹ Emma Timmins-Schiffman ⁴

¹Institute for Marine and Antarctic Studies, University of Tasmania, Hobart, Tasmania, Australia

Abstract

The influence of global change on Southern Ocean productivity will have major ramifications for future management of polar life. A prior laboratory study investigated the response of a batch-cultured subantarctic diatom to projected change simulating conditions for 2100 (increased temperature/CO₂/irradiance/iron; decreased macronutrients), showed a twofold higher chlorophyll-derived growth rate driven mainly by temperature and iron. We translated this design to the field to understand the phytoplankton community response, within a subantarctic foodweb, to 2100 conditions. A 7-d shipboard study utilizing 250-liter mesocosms was conducted in March 2016. The outcome mirrors lab-culture experiments, yielding twofold higher chlorophyll in the 2100 treatment relative to the control. This trend was also evident for intrinsic metrics including nutrient depletion. Unlike the lab-culture study, photosynthetic competence revealed a transient effect in the 2100 mesocosm, peaking on day 3 then declining. Metaproteomics revealed significant differences in protein profiles between treatments by day 7. The control proteome was enriched for photosynthetic processes (c.f. 2100) and exhibited iron-limitation signatures; the 2100 proteome exposed a shift in cellular energy production. Our findings of enhanced phytoplankton growth are comparable to model simulations, but underlying mechanisms (temperature, iron, and/or light) differ between experiments and models. Batchculture approaches hinder cross-comparison of mesocosm findings to model simulations (the latter are akin to "continuous-culture chemostats"). However, chemostat techniques are problematic to use with mesocosms, as mesozooplankton will evade seawater flow-through, thereby accumulating. Thus, laboratory, field, and modeling approaches reveal challenges to be addressed to better understand how global change will alter Southern Ocean productivity.

*Correspondence: philip.boyd@utas.edu.au

This is an open access article under the terms of the Creative Commons Attribution-NonCommercial License, which permits use, distribution and reproduction in any medium, provided the original work is properly cited and is not used for commercial purposes.

Additional Supporting Information may be found in the online version of this article.

†Present address: Aix Marseille Université, Université de Toulon, CNRS, IRD, MIO UM 110, Marseille, France

Author Contribution Statement: P.W.B., M.J.E., and B.L.N. designed the study, M.J.E. and S.E. conducted the chemical metrics, R.S. conducted the phytoplankton metrics, M.F. and P.W.B. conducted the foodweb metrics, B.L.N. and E.T.-S. carried out the proteomics analysis, and S.C.D. provided guidance on modeling simulations. P.W.B. led the manuscript preparation with inputs from all co-authors.

Climate change is altering ocean conditions in complex ways with concurrent changes in many biologically influential properties, termed drivers or stressors, including temperature, CO₂, nutrients, and irradiance (Doney 2010). These changes influence foodwebs from microbes to top predators (Pörtner et al. 2014). However, it is logistically challenging to incorporate both alteration of multiple drivers (mimicking future environmental conditions) and the inclusion of many trophic levels into climate change manipulation experiments (Boyd et al. 2018). To date, experiments have either focused on the effects of multiple drivers on a single species (e.g., Brennan and Collins 2015), on natural communities in 4-liter incubation vessels (Hoppe et al. 2013; Trimborn et al. 2017), or manipulation of one driver and its influence on a foodweb, often using large (up to 50,000 liters) mesocosms (Sommer and Lengfellner 2008; Riebesell et al. 2018). To date, only one study has investigated the effects of two anthropogenic drivers

²Department of Environmental Sciences, University of Virginia, Charlottesville, Virginia

³Research School of Earth Sciences, Australian National University, Canberra, Australian Capital Territory, Australia

⁴Department of Genome Sciences, University of Washington, Seattle, Washington

(temperature, acidification) on a coastal foodweb within an 1800-liter mesocosm (Nagelkerken et al. 2020). Given the urgent need to better understand the cumulative effects of global ocean change on biota (Bindoff et al. 2019), we must rapidly develop innovative approaches to investigate the effects of multiple drivers on marine food webs.

Research into global ocean change on Southern Ocean biota has revealed that at least five environmental drivers (temperature, CO₂, light, iron [Fe], and macronutrients [nitrate, phosphate, and silicate]) influence phytoplankton physiology (Deppeler and Davidson 2017). There is also evidence of interactive effects between drivers on phytoplankton cellular processes (Boyd and Brown 2015). The outcome of a laboratory culture study (Boyd et al. 2016) revealed that a subantarctic diatom had improved physiological performance under projected year 2100 conditions (increased temperature, CO₂, light, Fe, and decreased macronutrients). Statistical modeling pointed to altered temperature and Fe having the greatest influences on diatom physiological rates including growth, silicification, and nutrient acquisition. The outcome of this experiment, enhanced growth rates by 2100, was similar to projections in model simulations for Southern Ocean phytoplankton (increased productivity; Kwiatkowski et al., 2019; Laufkötter et al. 2015) by 2100 and beyond.

However, the underlying mechanisms for projected increases in productivity can differ between model simulations and laboratory experiments. In brief, in the parameterization of numerical models in CMIP6 (Climate Model Intercomparison Project, version 6) at the basin scale, Southern Ocean phytoplankton are typically light- and Fe-limited. In the simulated future ocean, enhanced stratification can reduce mixing relative to the euphotic depth and, therefore, may result in reduced light stress and hence increased net primary productivity (NPP, Bopp et al. 2013; Kwiatkowski et al. 2020). Other prior analysis of the drivers of Southern Ocean NPP in eight models (Laufkötter et al. 2015) points, in addition to irradiance, to factors including warming (seven of eight models), floristics/ecology (four of eight, bottom-up and top-down controls), and/or alleviation of Fe stress (five of eight). In contrast, in laboratory studies using diatoms, Toseland et al. (2013) and Boyd et al. (2016) reveal that warming, in addition to increasing growth rate, plays another more nuanced role (Boyd 2019). Warming partially offsets the requirement for nutrients like phosphorus (projected to be less abundant by 2100) in polar and subpolar diatoms (Toseland et al. 2013; Boyd et al. 2016). In the case of Fe, laboratory studies reveal that it also reduces the cellular silica quota relative to nitrogen in subantarctic diatoms upon Fe addition (Timmermans et al. 2004; Boyd et al. 2016). Several Earth System Models now incorporate variable phytoplankton nutrient (or Fe) stoichiometry to biomass (carbon), with elemental ratios varying under light and nutrient limitation, allowing aspects of these physiological effects and subsequent biogeochemical implications to be studied in future climate projections (Kwiatkowski et al. 2018).

There is a need to resolve the role of these different underlying physiological mechanisms in setting future Southern Ocean NPP. There are constraints to both laboratory and modeling experiments. The former has limited ability to extrapolate the findings derived from individual species to the Southern Ocean. For models, their parameterizations of physiology are often hindered by our current state of conceptual knowledge, limited observational data for model evaluation, and computational expense for extensive model sensitivity experiments. Both Laufkötter et al. (2015) and Kwiatkowski et al. (2020) discuss the need to improve Fe parameterizations in models, along with the ability to incorporate global ocean change effects on phytoplankton and their grazers. One way to approach this impasse is to investigate the response of the subantarctic phytoplankton community to global ocean change projected for this region for 2100. Conducting such a field experiment might also yield insights into how other trophic levels would respond to projected future oceanic conditions. Additionally, we can better understand global ocean change ecology through upscaling laboratory studies to field settings (Chown 2020). Here, we used shipboard-based 250-liter mesocosms in which we mimicked year 2100 subantarctic conditions (increased CO₂, temperature, Fe supply, underwater irradiance; decreased macronutrients; from model projections reported in Boyd et al. 2015) to assess the phytoplankton community response to environmental change, within the holistic setting of a pelagic foodweb. Although the effects of such cumulative change to phytoplankton processes were our primary focus, we also investigated the alteration of other components of the subpolar foodweb, such as heterotrophic bacteria and mesozooplankton, to future Southern Ocean conditions.

Methods and materials

Water mass characteristics of the study site

The subantarctic comprises ~50% of the areal extent of the open waters (i.e., ice-free) of the Southern Ocean (Banse and English 1997). Much of this region is high nitrate–low chlorophyll (HNLC) due to low Fe availability, resulting in a complex foodweb with diverse phytoplankton, microbial, and metazoan communities (Eriksen et al. 2018). The experiment was conducted onboard the RV *Investigator* over 7 d near the Southern Ocean Time Series (SOTS) site in March/April 2016, toward the end of the phytoplankton growth season (Weeding and Trull 2014). SOTS consists of deep ocean moorings (Schulz et al. 2012) near 46.8°S/142°E (Supporting Information Fig. S1).

Manipulation approach

A prior laboratory study (Boyd et al. 2016) employed a collapsed factorial design to both assess the cumulative effect of five drivers (temperature, CO_2 , light, Fe, and macronutrients) on cultured diatom species, and to differentiate the contributions of individual drivers to the cumulative outcome by using

wide-ranging metrics. In the present shipboard study, we simplified this design to two treatments: control (i.e., present day) and year 2100. We employed two 250-liter mesocosms on the ship rather than surface-tethered ones (Riebesell et al. 2018) due to the difficulties in deploying such structures in the Southern Ocean. Previous oceanic deployments in the subarctic Pacific resulted in compromised treatments from seawater exchange between the mesocosm and the surrounding waters due to mechanical damage (Takeda 1998). In addition, it is not possible to set up a five driver experiment in a surface-tethered mesocosm.

Shipboard mesocosms posed additional challenges in setting up the manipulations that we did not encounter in the parallel laboratory study (Boyd et al. 2016). The first challenge was to incorporate the requirement for reduced macronutrient concentrations in the 2100 treatment (Boyd et al. 2015). We overcame this issue by exploiting the voyage timing near the end of the phytoplankton growth season when surface macronutrients approach their annual minimum (Shadwick et al. 2015). We added nutrients to the "control" to provide (i.e., by difference) a "decreased nutrient" treatment for the 2100 mesocosm. The second issue to consider was how joint alteration of CO₂ (acidification) and dissolved Fe (acidification can alter Fe chemistry; Sunda and Huntsman 2011). The third hurdle was the need to collect >500 liters of seawater under trace metal clean conditions, while capturing a representative mesozooplankton community; some mesozooplankton evade capture unless sampled carefully (Santos et al. 2017).

Sampling and mesocosm set-up

Night-time sampling commenced on 28 March 2016 when unfiltered seawater was pumped from \sim 3 m depth using a trace-metal clean tow-fish. The device was mounted from a boom off the ship's midship beyond the ship's wake and towed at three knots. Seawater was pumped directly into 250-liter multi-layer polyethylene bags (Entapack) that had been trace metal cleaned prior to use. The mesocosms were located in a constant temperature (CT) laboratory (set to ambient temperature, 12.5°C) and both were filled simultaneously

using a two-way flow splitter linked to an all-plastic pump (A100, Wilden) with a trace-metal clean Teflon diaphragm and valves.

Manipulations

The two treatments were set up as batch cultures. The environment in the control treatment reflected ambient seawater with the exception of an amendment with ~20% more macronutrients (chelexed to minimize Fe contamination, see Table 1). Ambient ammonium was $0.18 \mu \text{mol L}^{-1}$ and was not amended. For the 2100 treatment, we used subantarctic projections for the Northern Southern Ocean province from the NCAR Community Earth System Model (CESM) following a high-emission climate change scenario (RCP8.5; Boyd et al. 2015) to alter temperature, pCO2, and dissolved Fe (Table 1). Fe was added, chelated with EDTA (ratio of 1:1.5 mol: mol, i.e., subnanomolar EDTA to prevent Fe precipitation in the initial chemical speciation, see later), to raise the background Fe level by 0.1 nmol L⁻¹ (see Supporting Information Fig. S2A). Dissolved Fe was 0.14 ± 0.01 nmol L⁻¹ in the mesocosms before Fe addition. Ambient DFe 0.061 ± 0.004 nmol L⁻¹ (Ellwood et al. 2020) indicating only minor cumulative contamination during water sampling, macronutrient additions, and filling of the mesocosms. The seawater in the 2100 mesocosm was warmed by 2°C, within the CT laboratory, using a 100-watt flexible heating coil (placed underneath the mesocosm, which was insulated from the CT laboratory floor), and temperature was monitored and controlled using a Habistat Digital Temperature Thermostat. Irradiance was provided by ATI aquarium lights (Sunpower T5 lamps) and attenuated with neutral density screening. Irradiance was $80 \pm 41 \ \mu \text{mol}$ photons m⁻² s⁻¹ (mean \pm standard deviation, n = 9 measurements) for the control mesocosm and $139 + 55 \mu \text{mol photons m}^{-2} \text{ s}^{-1}$ for the 2100 mesocosm. Our target irradiance (80 μ mol photons m⁻² s⁻¹) for the control was arbitrarily selected due to difficulties in calculating mean underwater irradiances for the mixed layer (Denman and Gargett 1983), and for the 2100 mesocosm was \sim 20% higher irradiance (96 μ mol photons m⁻² s⁻¹, using projections on

Table 1. A summary of the manipulations in the control and year 2100 treatments. The latter had increased temperature, CO₂, light, Fe, and decreased macronutrients relative to the control.

Ocean properties	Control	Year 2100	Notes		
Temperature (°C)	12.5±0.1	14.5±0.2	Year 2100 had elevated temperature		
pCO ₂ (ppmv)	403±31	625±46	Year 2100 had elevated pCO ₂		
Light (µmol photons m ⁻² s ⁻¹)	80±41	139±55	Year 2100 had increased irradiance		
Dissolved Fe (nmol L ⁻¹)	0.14±0.01	$0.24{\pm}0.01$	Year 2100 had added iron chelexed with EDTA		
Nitrate (μ mol L ⁻¹)	16.4±0.2	14.0±0.02	Control amended with \sim 20% more macronutrients (chelexed)		
Phosphate (μ mol L ⁻¹)	1.3±0.05	1.0±0.03	As for nitrate		
Silicate (μ mol L ⁻¹)	$2.3 {\pm} 0.02$	$1.8 {\pm} 0.02$	As for nitrate		

changes to the surface mixed layer depth from Boyd et al. (2015)). While we exceeded our target (139 vs. 96), this irradiance was unlikely to cause photoinhibition (Alderkamp et al. 2010). Our target pCO₂ for the 2100 mesocosm was 700 ppmv and attained by increasing the dissolved inorganic carbon (DIC) in the mesocosm. We added potassium carbonate (Ultrapure, SigmaAldrich) followed by the addition of ultra-pure HCl so that there was no change in alkalinity (initial Alk, 2279 μ mol kg⁻¹), but DIC was increased by ~110 μ mol kg⁻¹. In the 2100 treatment, pCO₂ was 625 ppmv (i.e., less than the target of 700 ppmv). Mesocosm pH was measured daily using the mCP dye technique (Liu et al. 2011).

Experimental set-up

Sampling took place at day 0, nominally set at 6 h after the mesocosms had been filled, after gentle agitation of the flexible mesocosm skin. A peristaltic pump subsampled seawater from each mesocosm for a wide-range of metrics: nutrients, chlorophyll, pCO₂, active fluorescence (using Fast Repetition Rate Fluorometry), Net Primary Production (using ¹⁴C), and Fe uptake (using ⁵⁵Fe). With the exception of heterotrophic bacterial production and sampling for mesozooplankton, all other methods followed long-established procedures (*see* references in Supporting Information Table S1). Statistical analysis of datasets presented in Figs. 1, 2, 7 used ANOVA and Tukey's

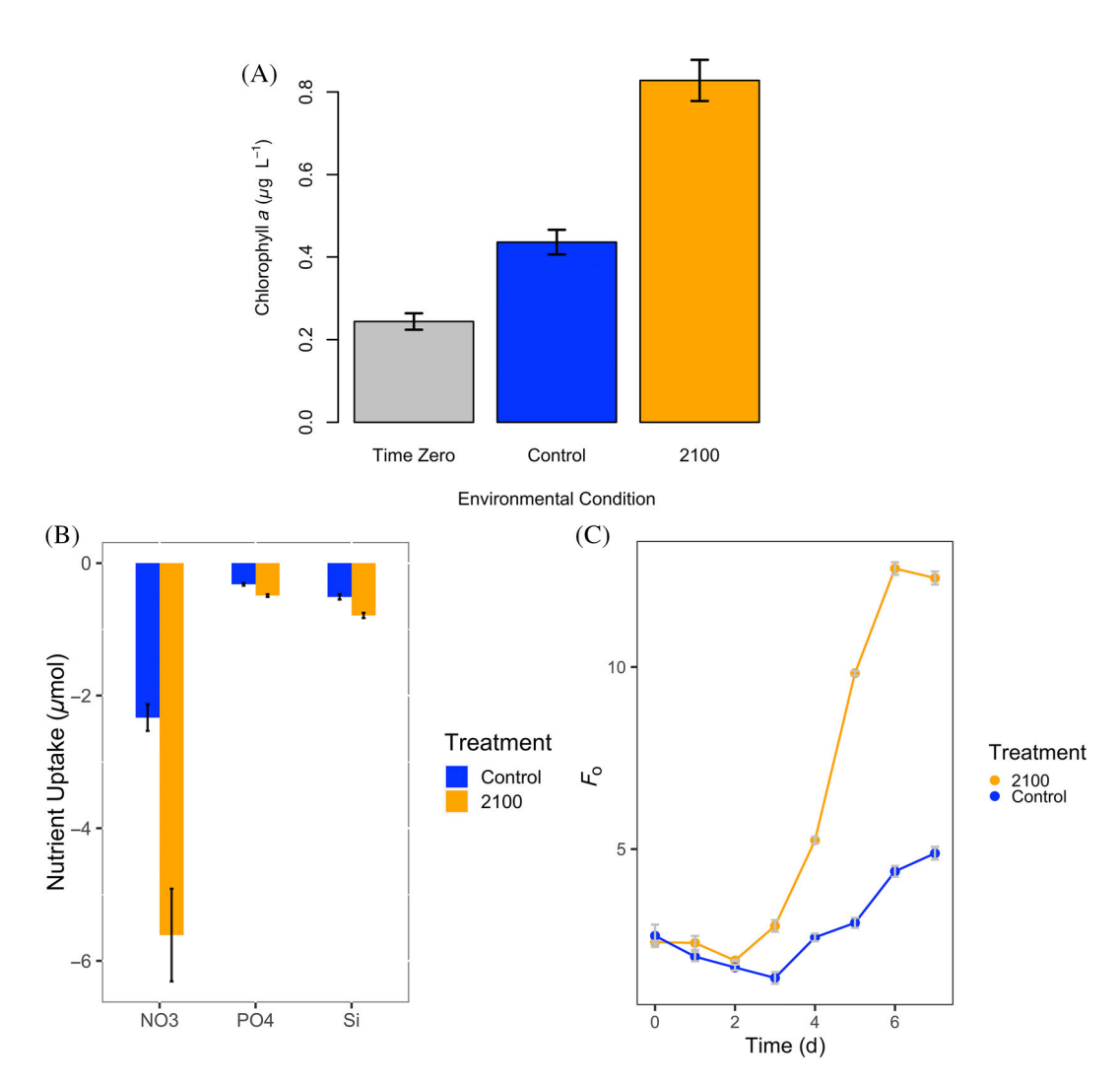


Fig. 1. (A) Extracted chlorophyll on days 0 and 7 in both mesocosms (error bars are standard error of the mean [n = 3], one-way ANOVA p = 1.71 e-06, see Supporting Information Data S1); (B) nutrient depletion for nitrate, phosphate, and silicate calculated by difference between days 0 and 7 nutrient concentrations (error bars are as for chlorophyll, Tukey's HSD nitrate p = 2.0e-07, phosphate p = 1.98e-04 and silicate p = 5.52e-05; (C) time series of initial fluorescence from active fluorescence (i.e., F_0) a proxy for phytoplankton stocks (error bars are as for chlorophyll, time-points from day 4 onwards were significantly different [Tukey's HSD, see Supporting Information Data S1]). Initial nutrient concentrations in each treatment are presented in Table 1. The (net) increases in chlorophyll equate to mean Fe requirements of 8.2 (0.2–30.8, min, max) pmol L^{-1} (control) and 25.6 (0.6–90.8, min, max, 2100) based on measured Chl a: Fe ratios (g mol $^{-1}$) from three Southern Ocean lab cultured species from Strzepek et al. (2012) and Strzepek et al. (2019). As herbivory may have accounted for the loss of \sim 90% of chlorophyll stocks, Fe requirements may have been >0.1 nmol L^{-1} and >0.03 nmol L^{-1} in the 2100 and control treatments, respectively (see Supporting Information Fig. S2).

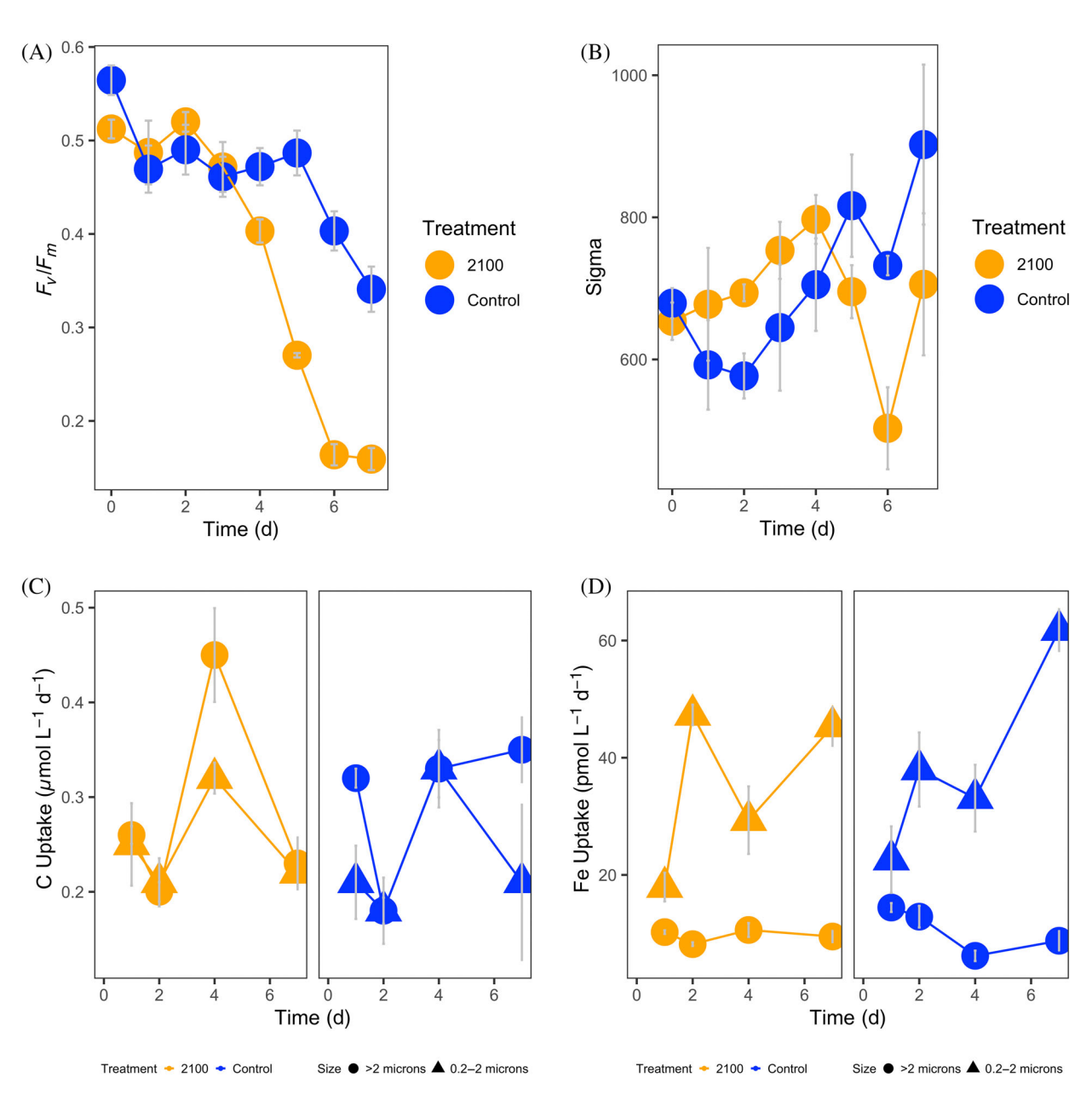


Fig. 2. Time series of (A) photosynthetic competence (F_v/F_m) from active fluorescence; (B) sigma, $σ_{PSII}$ (photochemical absorption cross-section of PSII, units nm² quanta⁻¹) from active fluorescence; (C) C uptake rates from ¹⁴C incorporation for two size fractions; (D) Fe uptake rates from ⁵⁵Fe incorporation for two size fractions. Error bars are standard error of the mean (n = 3). For panels (A) and (B), time-points from days 4 and 6 onwards, respectively, were significantly different (Tukey's HSD, *see* Supporting Information Data S1). For panels (C) and (D), there were no significant differences between treatments, *see* Supporting Information Data S1.

HSD (R Core Team 2013) is presented in Supporting Information Data S1. Due to difficulties in filtering large sample volumes, metaproteomics were performed on the >5 μ m fraction only. Thus, the proteome sampling will be skewed toward larger eukaryotic phytoplankton and will exclude some of the smaller size classes (e.g., coccolithophores and cyanobacteria). For the metaproteomics analysis (i.e., protein digestion and desalting, liquid chromatography-mass spectroscopy [LC–MS] and mass spectroscopy [MS]) and data transformations

(peptide identification and protein inference, metaGOmics: taxonomic and functional community proteomics analysis) presented in Figs. 3–6; *see* Supporting Information Data S1 (Methods follow Riffle et al. 2018 and Mikan et al. 2020).

Heterotrophic bacterial production was assessed using seawater collected in sterile 15-mL polycarbonate tubes during subsampling. Incubations commenced within 30 min of collection and were maintained at in situ temperature (12.5°C). The leucine incorporation method (with centrifugation) was

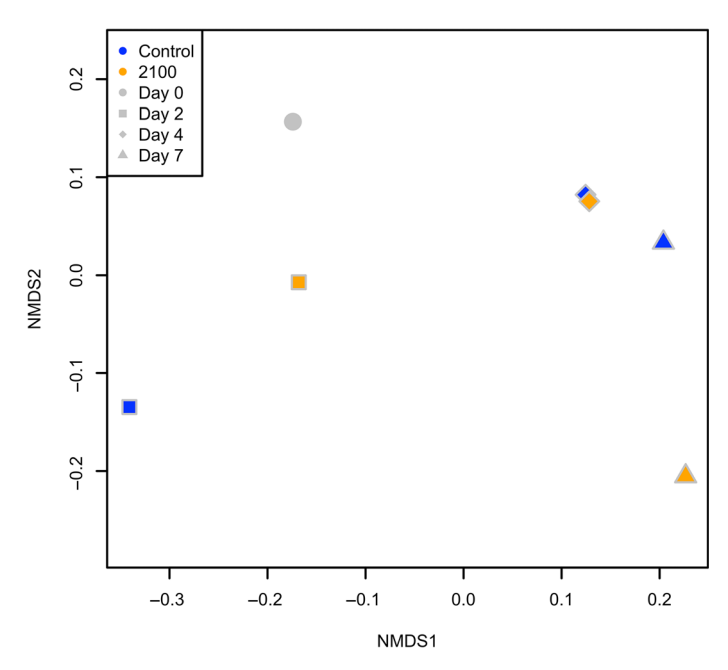


Fig. 3. Nonmetric multidimensional scaling plot (NMDS) of the entire metaproteomics dataset from phytoplankton >5 μ m (n=977 proteins). Symbols representing samples from control mesocosms are in blue and those from 2100 mesocosms are in orange across days 0 (gray circle), 2 (squares), 4 (diamonds), and 7 (triangles). Proteomic profiles did not differ significantly between individual days or between treatments.

used, along with conversion factors to obtain rates as μ g C L⁻¹ d⁻¹ following procedures in Fourquez et al. (2020). For higher trophic levels, metrics could only be sampled at the end of the experiment. Mesozooplankton, due to their ability to elude capture, were collected on day 7. Seawater within each mesocosm was filtered through a 200- μ m mesh, then the bag was cut open and all animals were washed off the walls using seawater and collected onto a filter. Mesozooplankton were examined using microscopy and then processed for particulate organic carbon (POC) analysis. The 7-d duration of the experiment was due to constraints imposed by the vessel's schedule.

Data availability

The physiological data presented in Figs. 1, 2, 7 in the Results section are available from the IMAS data portal (https://data.imas.utas.edu.au/). All metaproteomics data presented in Figs. 3, 4, 5 in the Results section are on the PRIDE ProteomeXchange repository (Deutsch et al. 2019; Perez-Ríverol et al. 2019) under the accession number PXD021185 (login reviewer44062@ebi.ac.uk and password SzXCx80Q).

Results

Initial conditions at the study site

The surface mixed layer at SOTS, just prior to filling the mesocosms (i.e., day 0), was $\sim\!100\,\mathrm{m}$ deep with some shallower density structure. The upper water column was characterized by 12.5°C temperature, 403 ppmv pCO₂, 1.0 μ mol

L⁻¹ phosphate; $14 \ \mu \text{mol L}^{-1}$ nitrate, and $1.8 \ \mu \text{mol L}^{-1}$ silicate. DFe was ~0.061 nmol L⁻¹ (range 0.057–0.064 nmol L⁻¹ from 15 to 70 m depth); chlorophyll was 0.23 $\mu \text{g L}^{-1}$, and despite the HNLC conditions, the photosynthetic competence (F_v/F_m) of the phytoplankton community was >0.5 and the photochemical absorption cross-section of PSII (σ_{PSII}) was >600 nm² quanta⁻¹. Based on metaproteomics, the phytoplankton community was a mixed assemblage including diatoms and dinoflagellates (data not shown), as is typically observed at the SOTS site (Eriksen et al. 2018). Microzooplankton were dominated by ciliates and flagellates (from microscopy, data not shown) were mainly amphipods and calanoid copepods.

Temporal trends in phytoplankton physiology

Chlorophyll was $0.23 \pm 0.02 \ \mu g \ L^{-1}$ on day 0 and by day 7 had increased to $0.42 \pm 0.03 \ \mu g \ L^{-1}$ in the control and $0.84 \pm 0.05 \ \mu g \ L^{-1}$ in the 2100 mesocosm (Fig. 1). Temporal changes in chlorophyll were tracked using the initial chlorophyll fluorescence from the FRRF, F_0 , as a proxy. F_0 was initially around 3 (arbitrary units), increasing fourfold in the 2100 mesocosm to 12 where it peaked after 6 d, whereas in the control it was maximal (>4) on day 7 (Fig. 1). Nutrient depletion also reflected these differences between the treatments, with nitrate depletion (over 7 d) of 2.3 μ mol L⁻¹ in the control (c.f. 5.6 μ mol L⁻¹, 2100 treatment); silicate depletion of 0.45 μ mol L⁻¹ (c.f. 0.55 μ mol L⁻¹, 2100 mesocosm), and $0.35 \mu \text{mol L}^{-1}$ phosphate depletion (0.42 $\mu \text{mol L}^{-1}$, 2100 mesocosm) (Fig. 1). The nitrate: phosphate (molar) drawdown ratios were \sim 7 in the control, but >10 in the 2100 treatment, driven by more nitrate relative to phosphate uptake under the 2100 conditions. The ratio of silicate: nitrate uptake was 0.2 in the control, slightly higher than for the 2100 mesocosm and indicative of relatively little diatom activity across the resident community that we sampled; ratios of ~ 1 and >> 1 are typical in a subpolar diatom-dominated community under Fe-replete and -deplete conditions, respectively (Boyd et al. 2005).

 F_v/F_m was initially relatively high given the HNLC conditions at SOTS, and the mesocosm time-series revealed two distinct trends. First, little change for the first 3 d then a marked decrease in the 2100 mesocosm reflecting a transient increase in F_o (Figs. 1C, 2A). The decline in F_v/F_m was much less pronounced in the control. Similar contrasting trends for F_o and F_v/F_m have been observed in other subpolar shipboard mesocosms (Strzepek unpublished data). σ_{PSII} was initially ~ 600 and increased to ~ 700 nm² quanta⁻¹ in both treatments by day 4 before increasing further in the control, and decreasing in the 2100 mesocosm (Fig. 2B).

Trends in community NPP and Fe uptake rates, and their size-partitioning are presented in Fig. 2. For NPP, in both treatments cells <2 μ m had lower rates than larger cells on day 4 in the 2100 mesocosm, and on day 7 in the control. Dark bottle ¹⁴C activity, often used as blanks for NPP using the ¹⁴C

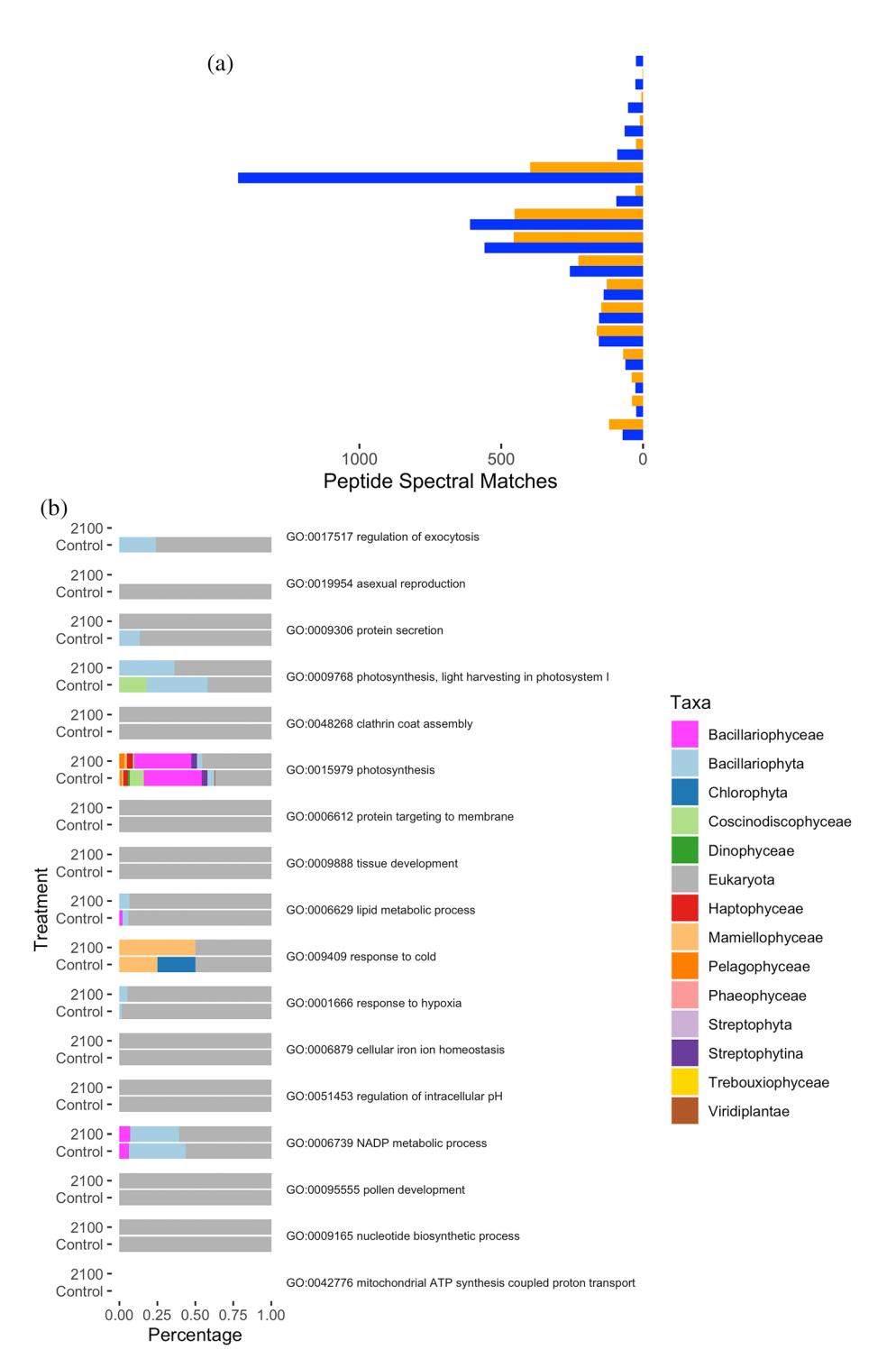


Fig. 4. MetaGOmics results for Gene Ontology (GO) terms that were significantly different between mesocosm treatments on day 7 for the >5 μ m phytoplankton. The bars on the left side of the plot in (b) represent the total peptide spectral matches (PSMs) for each GO term listed for (a) control (blue) and 2100 (orange) treatments. The stacked bars on the right part of the plot in (b) show the taxonomic contribution to the GO terms in the different mesocosms. Taxonomy is reported from the kingdom to class level; when taxonomy could not be resolved (the peptide sequence was too conserved across taxa), there is no bar representing taxonomy. Terms like "pollen development", "tissue development," and "response to hypoxia" are an artifact of the annotation process (see Supporting Information Data S1 for proteins included in the GO terms). For example, the phytoplankton proteins involved in "pollen development" are associated mainly with ATP production.

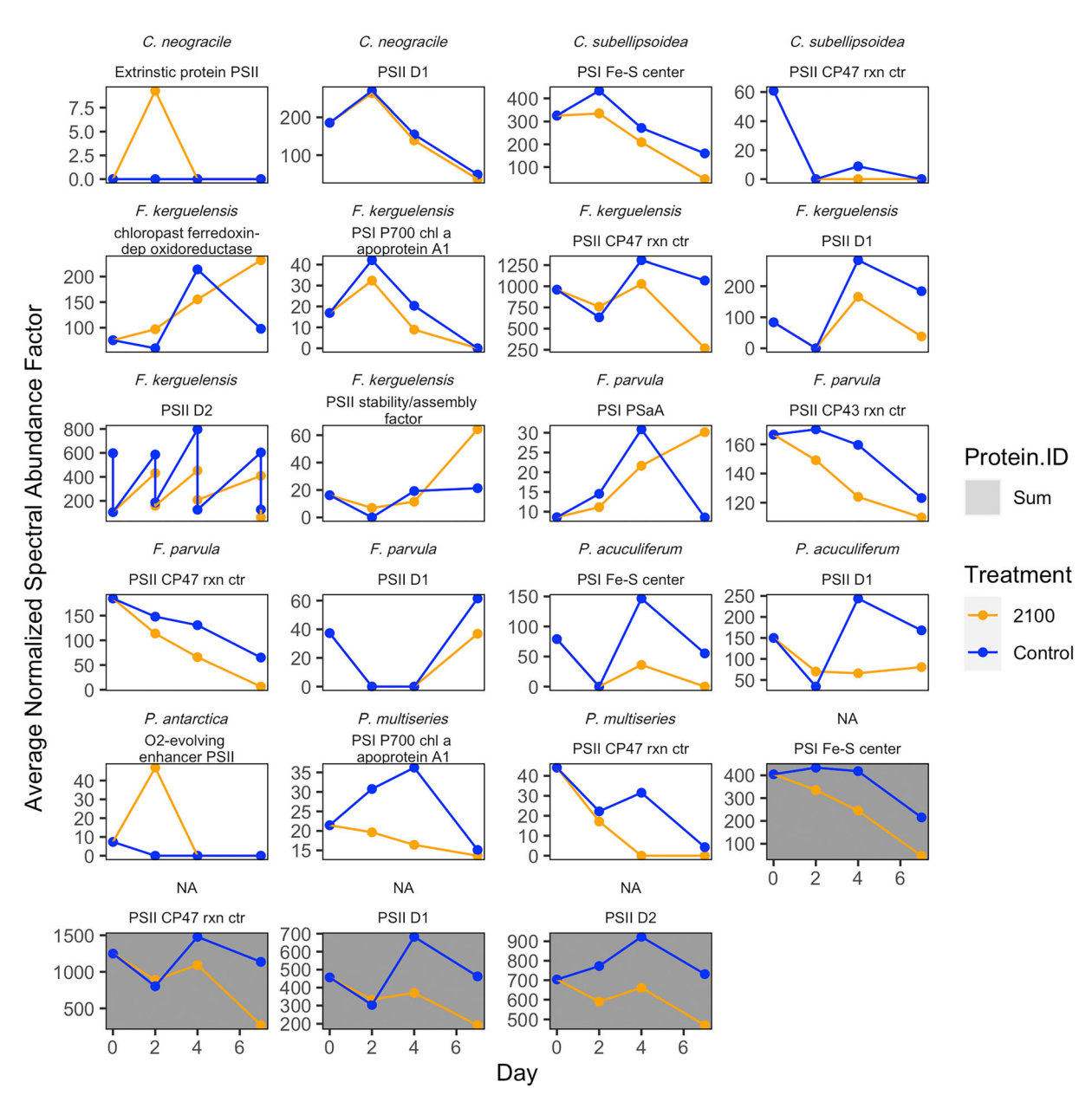


Fig. 5. Protein abundance for photosynthesis-related proteins for the >5 μ m phytoplankton across time points for control (blue) and 2100 (orange) treatments. Each plot panel represents a single protein identified in a single taxon. Plots with gray backgrounds are summed protein abundances across taxa for proteins that were identified in multiple taxa. *C. neogracile* = Chaetoceros cf. neogracile; C. subellipsoidea = Coccomyxa subellipsoidea; F. parvula = Florenciella parvula; F. kerguelensis = Fragilariopsis kerguelensis; P. acuculiferum = Peridinium acuculiferum; P. antarctica = Phaeocystis antarctica; P. multiseries = Pseudo-Nitzschia multiseries. PSI = photosystem I; PSII = photosystem II; Fe-S = iron-sulfur; rxn ctr = reaction center; dep = dependent; chl a = chlorophyll a.

approach but reflecting heterotrophic bacterial activity (Li 1982; Harris et al. 1989: Quero et al. 2020), was <10% of that in the light bottle 14 C activity (data not shown). Interestingly, the differences between treatments in chlorophyll accumulation (F_0) were not reflected by the NPP trends (Figs. 1, 2).

Community Fe uptake rates were comparable for both treatments, showing an increase from ${\sim}25$ to ${\sim}45~\text{pmol}~\text{L}^{-1}~\text{d}^{-1}$ from the initial time-point to those sampled on day 2, then a

slight decrease in each treatment for samples harvested on day 4. Uptake rates were slightly higher in the control by the final time point (Fig. 2D). Cells <2.0 μ m dominated Fe uptake in both treatments and drove trends in community Fe uptake. The uptake rates of larger cells were largely invariant over time.

The pH in the control (8.0) and 2100 (7.8) mesocosms altered Fe speciation such that Fe bioavailability and hence Fe uptake rates should be reduced at pH 7.8 (20–100% depending

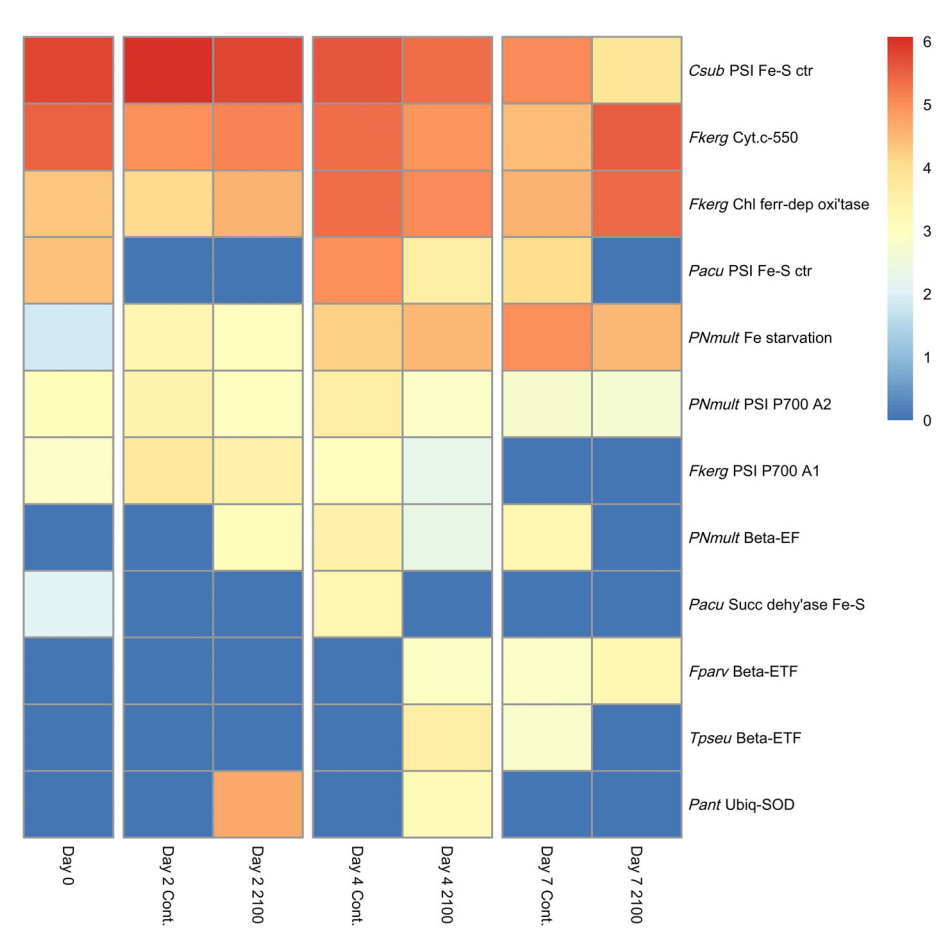


Fig. 6. Heatmap of the relative abundance of proteins, for the >5 μ m phytoplankton, dependent upon iron from day 0 to day 7 of the mesocosm incubation in Control and 2100 treatments. Colors in heatmap represent spectral counts for treatments that were $\log(x + 1)$ transformed. Protein names are listed on the right side of the figure and are sorted by maximum values. Csub = Coccomyxa subellipsoidea; Fkerg = Fragilariopsis kerguelensis; Pacu = Peridinium acuculiferum; PNmult = Pseudo-Nitzschia multiseries; Fparv = Florenciella parvula; Tpseu = Thalassiosira pseudonana; Pant = Phaeocystis antarctica; PSI = Photosystem I; PSII = Photosystem II; PSII = PSII = Photosystem II; PSII = PSI

on Fe species, i.e., enough to offset increased Fe in the 2100 treatment) compared to pH 8.0 (Hudson et al. 1992; Sunda and Huntsman 2003; Shi et al. 2010). Interestingly, there was no discernible difference in Fe uptake rates between treatments, potentially due to changes in organic Fe complexation associated with ligand production. Community Fe : C uptake ratios ranged from 52 to 145 μ mol : mol (60–145 [control]; 52–135 [2100]), with no evidence of temporal trends in either mesocosm. Ratios were 19–73 for the >2 μ m fraction and 73–290 for the <2 μ m fraction with no clear differences between mesocosms.

Temporal trends in phytoplankton metaproteomics

There were 977 proteins, from the >5 μ m phytoplankton fraction, with at least two unique peptides across the experiment inferred from mass spectrometry. On a whole community proteome scale, mesocosm metaproteomes were not significantly different by day or treatment (Fig. 3; ANOSIM p-value > 0.05); however, there were significant shifts in

individual proteins and classes of proteins in a more detailed analysis (*see* below). Here, we explore the results and their implications for the experimental outcomes.

There is evidence of physiological acclimation by resident phytoplankton in the >5 μ m size fraction to the mesocosm conditions; Non-metric multidimensional analysis of the matrix of proteins quantified across the incubation time-line illustrates how the proteomes are significantly different between treatments on day 2, converge on day 4 and then diverge on day 7 (Fig. 3) for the >5 μ m size fraction of phytoplankton. The distinct shift in the metaproteomic profile that occurred between days 2–4 is also reflected in the relative abundances of taxonomic groups throughout the incubation (Data not shown). By day 7, there is a significant separation between the control and 2100 treatments reflecting distinct responses to each treatment (Fig. 3).

The MetaGOmics analyses included a biological enrichment analysis of identified peptide quantities associated with Gene Ontology (GO) terms (Fig. 4). MetaGOmics identified

significant changes in the quantified peptides' taxonomic and functional assignments of the two treatments on day 7. GO terms that were statistically enriched (p < 0.01) under control conditions (c.f. 2100) included those involved in photosynthesis (including enrichment in the generic terms "Photosynthesis. harvesting photosystem in "Photosynthesis"), protein assembly and export (including enrichment in the generic terms "Regulation of exocytosis," "Protein secretion," "Clathrin coat assembly," and "Protein targeting to membrane"), and environmental sensing (including enrichment in the generic terms "Response to cold," "Response to hypoxia," and "Cellular Fe ion homeostasis"). Additionally, the following individual terms were also significantly enriched: "Lipid metabolic process," "Asexual reproduction," and "Tissue development." The higher abundances of photosynthesis-related peptides (from photosystem and light-harvesting proteins, among others) suggest increased activity of photosynthetic processes in the control towards the day 7. Additional proteomic evidence suggests that the $>5 \mu m$ phytoplankton in the control used this increased energy production from photosynthesis, with evidence of increases in proteins related to protein production (e.g., protein transport protein SEC23), lipid metabolism (e.g., acetyl-CoA enzymes), and possibly cellular growth (e.g., cell division protein CDC78CY).

An increased demand for cellular energy production for the > 5 μ m phytoplankton in the 2100 mesocosm was evidenced by the higher representation of GO terms (and contributing proteins) related to energy production. This was highlighted by the inclusion of V-type proton ATPase, chaperones, ATP synthase, eukaryotic initiation factor, and catalase in the enrichment of GO terms such as "mitochondrial ATP synthesis coupled proton transport" and "NADP metabolic process" (Fig. 4). In addition, other GO terms that were more abundant in the 2100 mesocosm were "Regulation of intracellular pH," "Pollen development," and "Nucleotide biosynthetic process." Many of these peptides and their associated processes are involved in energy production since ATPase and ATP synthase were indicated for most GO terms.

Temporal trends in the abundance for photosynthesis-related proteins (Fig. 5) were analyzed in order to correlate omic data with the different trends in photophysiology (F_v / F_m , F_o , σ_{PSII}) between the mesocosms (Figs. 1, 2). Some proteins followed similar trends in the two treatments (e.g., Photosystem II D1 protein from C. neogracile), but the relative abundance of other proteins diverged between the mesocosms. The photosynthetic protein data are indicative of a photoacclimation signature, in particular due to the photosystem proteins being enriched in the control treatment with a lower irradiance compared to 2100. The temporal trends are more divergent and therefore difficult to interpret. In many cases, the peak followed by a decline (upper panels in Fig. 5) is consistent with the transient shifts in the photophysiological metrics. In other examples from Fig. 5, such as the multiple

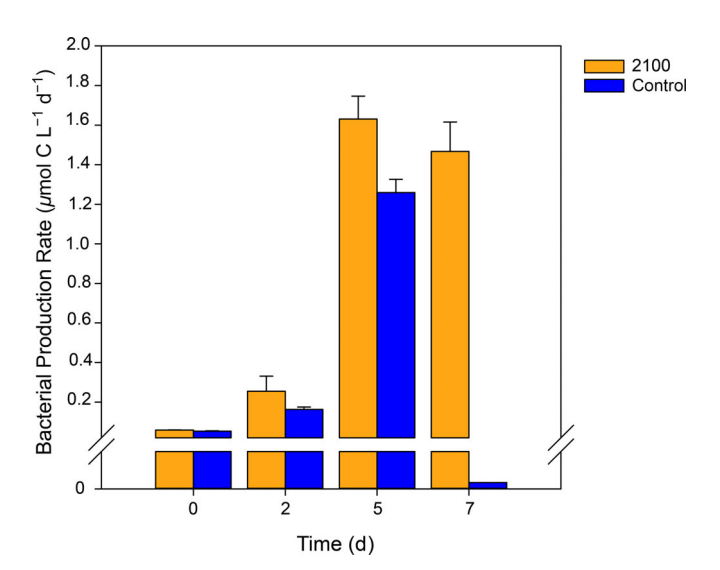


Fig. 7. Time series of heterotrophic bacterial production upscaled from 2 h incubations to daily rates and converted from leucine incorporation to C uptake. On day 7 in the control bacterial production was 2 ± 1 nmol C L⁻¹ d⁻¹. Error bars denote the standard error of the mean (n = 3). Timepoints from day 2 onwards were significantly different (Tukey's HSD, *see* Supporting Information Data S1).

panels for PSII D1, it is difficult to reconcile the diverse taxon-specific trends with the community-based photophysiology datasets that integrate the effects of taxonomy (Suggett et al. 2009), mesocosm irradiances (Strzepek et al. 2012), and nutrient availability under batch-culture conditions (Parkhill et al. 2001).

As SOTS is within a low Fe HNLC region (Ellwood et al. 2020), and as there were differences in initial DFe concentrations and bioavailability between treatments, we focused on the relative abundance of proteins, for the >5 μ m phytoplankton, dependent upon Fe from days 0-7. Several of the significantly different GO terms are related to cellular Fe use (Fig. 4). Smaller organisms dominated Fe uptake, but our analysis of cells $>5 \mu m$ means we did not measure peptides from these small-celled taxonomic groups. Some Fe-requiring proteins decreased in abundance by day 7 in the 2100 mesocosm, but not in the control, are likely due to the greater accumulation of enhanced Fe-rich phytoplankton biomass in the latter (see Fig. 1 caption). They included Photosystem I Fesulfur center (PSI Fe-S ctr proteins from C. subesllipsoidea and P. acuculiferum), electron transport flavoprotein subunit beta (Beta-ETF proteins from P. multiseries and T. pseudonana), and succinate dehydrogenase ubiquinone Fe-S subunit (Succ dehy'ase F-S proteins from P. acuculiferum) (Fig. 6). Other proteins exhibited dynamic changes over time and across treatments (e.g., Photosystem I P700 Chlorophyll a and apoprotein A1, F. kerguelensis). Interestingly, the Fe starvationinduced protein (P. multiseries) increased in abundance on day 7 in both mesocosms, consistent with Fe limitation whereas by day 7 photosynthetic competence indirectly exhibited Fe

limitation in the 2100 treatment, but Fe limitation was less evident in the control mesocosm (Fig. 6 c.f. Figure 2A).

Trends in foodweb processes

Heterotrophic bacterial production increased \sim 20-fold in both treatments, with the initial increase (day 2) being greatest in the 2100 mesocosm followed, with a slight lag, by the control (Fig. 7). After day 5, there was a "crash" in rates (c.f. Fourquez et al. 2020) in the control indicative of resource limitation; the decline was much less pronounced in the 2100 mesocosm. Mesozooplankton stocks on day 7 were not significantly different between mesocosms (10.2 [control] vs. 11.5 mg POC m $^{-3}$ [2100]) and were calanoid copepods and amphipods similar to those from net hauls at SOTS in March 2018. Day-0 sampling for mesozooplankton was not possible from the tow fish and so mesocosm stocks were compared with those from other HNLC subpolar regions (Bradford-Grieve et al. 1998; Goldblatt et al. 1999) and were similar to reported late summer biomasses.

Herbivory by meso- and micro-zooplankton was estimated indirectly using the approach of Moreau et al. (2020) that compares the intrinsic (i.e., independent of grazing) metric of nitrate uptake with that of an extrinsic grazer-dependent metric (chlorophyll accumulation). The ratios for chlorophyll accumulation: nitrate drawdown (µg: µmol) were 0.09 (control) and 0.11 (2100). In contrast, the ratio averaged across the evolution, peak, and decline of Southern Ocean blooms (i.e., negligible herbivory) was ~1.0 (sta. 29/57, Supporting Information Table S1, Moreau et al. 2020), which suggests pronounced grazing in the mesocosms, typical of HNLC (Steinberg and Landry 2017) and Southern Ocean waters (Moreau et al. 2020). Using this ratio of 1.0 suggests that for nitrate consumption in each mesocosm \sim 2.3 and 5.6 μ g chlorophyll L⁻¹ was synthesized within the control and 2100 treatments, respectively. This compares with measured chlorophyll increases of 0.20 (0.43–0.23 $\mu g L^{-1}$, control) and 0.59 $(0.82-0.23 \ \mu g \ L^{-1}, \ 2100, \ Fig. \ 1)$. Thus, herbivory may have removed >90% (i.e., 0.2 [observed] c.f. 2.3 [theoretical] µg Chl $a L^{-1}$) and ~90% (0.59 c.f. 5.6 µg Chl $a L^{-1}$) of stocks in the control and 2100 treatments, respectively.

Discussion

In our two treatments, we mimicked environmental conditions projected for 2100 and the present day (albeit with macronutrient additions to the "control") for subantarctic waters and captured a representative mesozooplankton community. Thus, we were able to extend the parallel laboratory study of Boyd et al. (2016) to a phytoplankton community within a subpolar pelagic foodweb in a mesocosm. Here, we consider the initial conditions of the experiment, then explore the insights provided by phytoplankton physiological and proteomic responses to the 2100 manipulation prior to discussing foodweb responses. We conclude with a critique of the

transition from laboratory to field settings for manipulation experiments and compare our findings with those of model simulations of future Southern Ocean NPP.

Initial conditions

Nutrients, Fe, and chlorophyll concentrations reflected late season conditions at this HNLC site (Ellwood et al. 2020). One puzzling characteristic was the photosynthetic competence (>0.5) and σ_{PSII} (<700 nm² quanta⁻¹) of the resident phytoplankton, which are more typical of Fe-replete cells in the polar (Boyd and Abraham 2001) and subantarctic (Boyd et al. 1999b) Southern Ocean. One explanation of the σ_{PSII} and F_{ν}/F_{m} values is that the predominance of small cells within a mixed phytoplankton community, often observed at SOTS (Eriksen et al. 2018), may have had a disproportionate influence on these metrics (see Suggett et al. 2009); small phytoplankton have high surface area: volume ratios, which aids Fe acquisition relative to cellular demand (Lis et al. 2015). The elevated F_v/F_m of the subantarctic community must be carefully considered in the interpretation of the mesocosm datasets.

Response of phytoplankton to 2100 conditions

Our aim was to assess the phytoplankton response to future oceanic conditions, within a pelagic foodweb setting. Phytometrics fall into two categories, (e.g., nutrient uptake) and extrinsic (e.g., chlorophyll concentrations) responses that provide insights into the relative roles of environmental vs. ecosystem controls on the mesocosms. Together, intrinsic and extrinsic metrics provided coherent trends, such as increased F_0 , nitrate depletion, and chlorophyll concentrations that showed distinctive differences between treatments (Fig. 1). These trends were also evident to a lesser extent for phosphate depletion. The temporal trends between treatments for intrinsic metrics such as F_v/F_m , NPP and Fe uptake were more difficult to intercompare and interpret as F_{ν}/F_{m} and NPP suggested that phytoplankton growth led to Fe limitation in the 2100 treatment by the end of the experiment (Fig. 2A,C), but there was the confounding influence of heterotrophic bacteria (Fig. 2D) on trends in community Fe uptake (Adly et al. 2015; Quero et al. 2020).

Intrinsic metrics such as nutrient uptake ratios reveal differences between the treatments. Higher N : P uptake ratios in the 2100 (>10 [less P uptake relative to N], c.f. 7.5 in the control mesocosm, were indicative of the potential role of temperature in physiologically mitigating lower phosphate supply, reported in laboratory manipulation studies on Southern Ocean phytoplankton (Toseland et al. 2013; Boyd et al. 2016). However, there was no evidence in the metaproteomic dataset (from >5 μ m phytoplankton) of a decrease of phosphorus-rich macromolecules (ribosomal RNA) used in protein translation. Such proteins are highly homologous across all kingdoms, which could have masked trends in the phytoplankton across the treatments.

During the incubation, there was evidence that the phytoplankton community in the 2100 treatment exhausted a limiting resource (probably Fe, see Fig. 1 caption) after 7 d. We observed an increase in Fo, a peak in NPP and a concurrent decrease in $F_{\nu}/F_{m\nu}$ after 3 d (Fig. 2). Similar transient responses in photosynthetic competence have been observed in shipboard mesoscosm studies in New Zealand offshore waters (Ellwood et al. 2015; Meyerink et al. 2019). Signatures that later reflect this initial period of enhanced physiological activity, nutrient drawdown and chlorophyll (with the caveat of grazing), were greatest on day 7. The response within the control was slower and more attenuated. Consequently, we sampled a population for proteomics that was more in decline for the 2100 treatment compared to the control. There was evidence of acclimation to the different environmental conditions in each mesocosm between days 2 and 4, and also a pronounced increase in Fe uptake within the first 48 h (i.e., incubation on day 1 of 24 h duration) driven by cells $<2 \mu m$, which was sustained throughout.

As expected, metaproteomics provided much greater detail than is possible from physiological metrics. These differences result from physiological measurements being made mainly at the community level preventing direct comparisons to higherresolution taxonomically resolved changes in protein abundance. Iron uptake was estimated in two size fractions, which offered insights into patterns within the phytoplankton community; however, the $<2 \mu m$ fraction also included heterotrophic bacteria taking up an unknown fraction of Fe. Trends in Fe-related proteins (conducted on the $>5 \mu m$ fraction only) suggested that Fe-requiring metabolic processes were greater in the 2100 mesocosm, but no significant difference was detected in Fe uptake rates by cells >2 μ m between the two treatments. At the species level, metaproteomics showed trends, in many cases, that were consistent with photoacclimation (to higher irradiance) in the 2100 treatment that mirror trends in the photophysiology for both treatments.

Trends in extrinsic metrics provide insights into ecosystem effects on the mesocosms. Despite high grazing pressure (\sim 90% of phytoplankton stocks), it did not mask the clear differences between the treatments as reflected by $F_{\rm o}$, chlorophyll accumulation and to a lesser extent NPP. Thus, it appears that environmental influences were more pronounced than ecological effects over the experiment. However, the effects of altered conditions on other trophic levels could not be assessed directly for grazers. Mesozooplankton stocks on day 7 were comparable in both treatments, and similar to those observed in other subantarctic waters (Bradford-Grieve et al. 1998). The experimental duration was too short to capture significant changes in mesozooplankton stocks (Boyd et al. 1999a).

The pronounced increase in heterotrophic bacterial production in both treatments was such that it exceeded community NPP by day 4 (Supporting Information Fig. S2). Day 0 bacterial production rates are comparable to those made several days

earlier at SOTS on the 2016 voyage (Fourquez et al. 2020), and by Church et al. (2000) in subantarctic waters south of Australia. The 20-fold increase in bacterial production in both treatments suggests that the influence, either individually or cumulatively (i.e., including interactions), of the five drivers we manipulated was not directly responsible for the increase. However, prior manipulation experiments in 0.5-liter (Fourquez et al. 2020) and 2-liter (Church et al. 2000) bottles, adding DFe and/or dissolved organic carbon (DOC, using glucose as a proxy) to resident heterotrophic bacteria both led to 20-fold increases (c.f. Fig. 7) in bacterial production driven by Fe/glucose (Fourquez et al. 2020) or glucose (Church et al. 2000). In both studies, Fe addition resulted in little change to rates of bacterial production.

In the present study, there was a marked and sustained increase in Fe uptake by cells $<2 \mu m$ after day 1 in both mesocosms. This pronounced increase may reflect the needs of heterotrophic bacteria, who along with pico-eukaryotes comprise stocks $<2 \mu m$. However, increased bacterial production did not scale with Fe uptake by $<2 \mu m$ cells (Supporting Information Fig. S2). Also, the observation that bacterial production (with the caveat that it was upscaled from 2 h incubations to 24 h) exceeded community NPP must also be reconciled. Increased bacterial production, based on the outcomes of the Fourquez et al. (2020) and Church et al. (2000) studies, suggests a marked increase in labile DOC, such as the exudation of photosynthate. Also, the distinct crash in bacterial production on day 7 (Fig. 7 caption) points to resource limitation. However, as we have no data on DOC concentrations in the mesocosms we cannot explore this speculation further. It is unlikely that increased bacterial production was fuelled by increased NPP in conjunction with enhanced phytoplankton DOC exudation, unless rapid DOC recycling is invoked. Estimated grazing of ~90% of phytoplankton stocks might accentuate recycling. Alternatively, it is possible that elevated bacterial production in both treatments is indicative of an escape from bacterivory and/or some artifact, such as colonization of mesocosm walls associated with 7 d of containment.

What do physiology and omics metrics jointly reveal?

Our experimental design was a simplified version of a parallel laboratory manipulation (Boyd et al. 2016) that provides the cumulative response to projected future ocean conditions. Using metaproteomics, we have uncovered evidence of physiological pathways downstream of, and parallel to, photosynthesis that may be important biomarkers of global ocean change. These pathways include protein export, environmental sensing (Fe, oxygen, temperature, and intracellular pH regulation via ATP proton pumps). Peptides associated with the pathways of protein export, environmental sensing, and regulation of exocytosis were detected at increased levels in the control, relative to the 2100 treatment for the >5 μ m phytoplankton. Southern Ocean phytoplankton have evolved several mechanisms to physiologically acclimate to conditions of

low ambient light, Fe concentrations, and temperature (Strzepek et al. 2019) and to resist damage from UV radiation. For the latter, resident phytoplankton have a high diversity of antioxidant defense mechanisms to maintain cellular integrity (Lyon and Mock 2014). Such mechanisms can be leveraged whenever cellular metabolism produces too many reactive oxygen species, whether due to metabolic up-regulation or stress. In our study, peptides of the antioxidant protein catalase were at increased levels in phytoplankton within the control mesocosm, as were chaperones (including many heat shock proteins, HSPs), and eukaryotic initiation factors. The abundance of catalase and HSPs suggests that the phytoplankton are responding to a physiologically-damaging environment (likely Fe limitation, see Supporting Information Fig. S2) by protecting essential cellular functions.

Comparing proteomic results from other studies of batch cultured Southern Ocean phytoplankton in response to Fe

limitation to our study revealed several similar metabolic responses (Table 2). A host of proteins, involved in making and exporting proteins from the endoplasmic reticulum and Golgi network, are associated with peptides at increased abundance in the control mesocosm, suggesting an increase in protein synthesis and endo-/exo-cytosis. A comparable trend was seen in Fe-limited diatoms (Nunn et al. 2013) and in a parallel laboratory manipulation of the diatom Pseudonitzschia multiseries (Boyd et al. 2016). As was proposed by Nunn et al. (2009) and Coale et al. (2019), increased presence of proteins related endo-/exo-cytosis suggests that the cell may be utilizing clathrin coated vesicles to transport in larger macromolecules, such as Fe-bound siderophores, rather than generating a range of membrane-bound transporter proteins that have specific targets. In our incubation study, these peptides associated with protein production are a signature of a change in physiological needs under low Fe on day 7.

Table 2. Comparison between the present study and recent Southern Ocean studies in which environmental manipulation studies were performed, and in which molecular and physiological tools were used to interpret the manipulations. Agreement with omics results refers to a comparison between the findings of these other published studies with the control and 2100 treatments in our study.

Trend observed	Species	Agree with omics?	Variables	Lab or ship	Location collected	Environmental or lab strain	Source
Increase PSI pathway, PSII genes	Fragilariopsis kerguelensis	Yes—control	Low Fe/low light	Lab	Atlantic Sector of the SO (48°S, 16°W)	Lab strain	Moreno et al. (2020)
Flavodoxin and ferredoxin detected	Nine species of diatom	Yes	Low Fe	Lab	Western Antarctic Peninsula along the Palmer LTER sampling grid	Environmental	Moreno et al. (2018)
Stimulated photosynthesis and growth	Phytoplankton community	Yes	+Fe	Ship	Ross Sea Poly nya	Environmental	Alderkamp et al. (2019)
Increased cell counts	Phytoplankton community	Yes	Warming +Fe	Lab	McMurdo Sound	Environmental	Jabre et al. (2021)
Photosynthetic competency lower	Fragilariopsis kerguelensis	No	Low Fe	Lab	Atlantic Sector of the SO (48°S, 16°W)	Lab strain	Moreno et al. (2020)
Photosynthetic apparatus proteins decreased	Phaeocystis antarctica	No	Low Fe/low light	Lab	McMurdo Sound	Lab strain	Wu et al. (2019)
Increased growth rate	Fragilariopsis cylindrus	Yes	Warming +Fe	Lab	Weddell Sea	Lab strain	Jabre and Bertrand (2020)
Photosynthetic efficiency low; increased sigma of PSII	Fragilariopsis cylindrus	Yes—2100	Warming + low Fe	Lab	Weddell Sea	Lab strain	Jabre and Bertrand (2020)
Reduction in PSII reaction centers	Fragilariopsis cylindrus	Yes	Warming	Lab	Weddell Sea	Lab strain	Jabre and Bertrand (2020)

In the 2100 mesocosm, there was an increase in detected peptides associated with the GO term "Regulation of intracellular pH" mainly associated with proteins such as ATP synthase and v-type proton ATPase. This detected physiological shift may be due to photoacclimation (Petrou et al. 2016) and/or a response to a change in environmental pH. Since there was higher irradiance and Fe supply in the 2100 mesocosm, the efficiency of photosynthesis may have increased, thus generating more protons to drive ATP synthase and up-regulating the production of ATP synthase complexes (Nunn et al. 2013). A similar trend was seen for *P. multiseries* incubated under comparable year 2100 conditions (Boyd et al. 2016). V-type proton ATPases hydrolyze ATP in the vacuole that drives a proton gradient to run various intracellular processes. An increase in V-type proton ATPases may signal an up-regulation of cellular trafficking (i.e., a signal of increased movement of molecules across the cellular membrane) and metabolism in conditions more favorable to photosynthesis. Many photosystem proteins were at relatively lower abundances in the 2100 mesocosm compared to the control. This trend could be due to an up-regulation of photosystem protein production in the control to compensate for photosynthetically unfavorable conditions, as also seen in Moreno et al. (2020) or resulting from down-regulation of photosystem proteins due to higher irradiance (Table 2). Additionally, the elevated pCO₂ (decreased pH) in the 2100 mesocosm may have stimulated an increase in enzyme-driven, as opposed to more passive, H⁺ efflux to maintain intracellular pH (Raven and Smith 1974; Taylor et al., 2011), a function attributed to Vtype proton ATPase (Toei et al., 2010).

Although no other study that we are aware of has examined the cumulative effect of altering Fe, light, CO₂, temperature and nutrients on a Southern Ocean pelagic community, others have looked at subsets of these manipulated parameters such as Fe and light. We cross-compared our findings to explore whether we can obtain insights into the individual environmental factors we manipulated (Table 2). The proteomic trends we observed in the photosystem I pathway in the control mesocosm are corroborated by previous work (Moreno et al. 2020). We also detected flavodoxin and chloroplast ferredoxin dependent NADH oxidoreductase proteins in some taxa. Although flavodoxin and ferredoxin have been detected in subpolar plankton communities (Boyd et al. 1999b; Moreno et al. 2018); we did not observe the trend of flavodoxin replacing ferredoxin in low Fe environments et al. 1999b). The absence of these proteins in our dataset may be due to the low biomass of our diverse natural community, which prevented us from detecting all translated proteins with high confidence. The convergent responses we see between our study (both treatments) and other published manipulation experiments, with the caveat that they manipulated fewer properties, suggests an important role of Fe and irradiance in controlling many aspects of phytoplankton physiology.

In other processes, we see divergent outcomes from our mesocosm study compared to those presented in Table 2.

Others detected that phytoplankton photosynthetic competency and photosynthetic apparatus proteins decrease under low Fe alone (Wu et al. 2019; Moreno et al. 2020); we observed the opposite trend. In our manipulation, five environmental drivers were altered, whereas in experiments against which we compare our results, one or two drivers were amended. A comparison of our study with a parallel 2100 laboratory manipulation (Boyd et al. 2016) reveals little evidence across the resident phytoplankton community for trends related to warming. In particular, there was no evidence of a decrease of phosphorusrich macromolecules (ribosomal RNA) used in protein translation in the 2100 mesocosm, even though we observed a decrease in the phosphate depletion relative to nitrate. The lack of corroboration may be due to P depletion reflecting all size classes across the phytoplankton community, whereas the metaproteomics targeted cells $>5 \mu m$.

Critique of the transition from laboratory to field settings

A major drawback to laboratory culture manipulations is that they often target one phytoplankton species. Thus, while this can enable the dissection of underlying mechanisms driving responses to global ocean change (Boyd et al. 2016), little can be reported on the wider ecological ramifications. We can assess the benefits and challenges of transitioning laboratory experiments to the field by comparing our study with Boyd et al. (2016). We successfully extended Boyd et al. (2016) to a subpolar phytoplankton community within a pelagic foodweb in a mesocosm. The primary challenge for mesocosm experiments is that prior to day 0, no ready assessment can be made on the environmental history of the community (termed here "line-of-sight"), whereas laboratory culture approaches allow for specific timing of acclimation to pre-selected environmental conditions.

Obtaining such a "line-of-sight" for HNLC waters should not have been problematic given the often reported "constancy of conditions" (see Strzepek et al. 2005). However, the initial high F_{ν}/F_{m} in HNLC waters was not anticipated, and also there are difficulties in mimicking underwater light climate as it requires rates of vertical mixing (Denman and Gargett 1983). The lack of a "line-of-sight" into accurate mimicry of conditions probably also resulted in acclimation (Fig. 4) during the shipboard manipulation, which has also been reported during Arctic oceanic manipulation studies (Hoppe et al. 2017). Such acclimation may have truncated the time period over which the resident cells could respond to the altered conditions. Acclimation also may have coincided with the transition to resource limitation evident after day 3 in the 2100 mesocosm with ramifications for the magnitude of the signals detected by physiological and metaproteomic approaches. For example, the parallel experiment of Boyd et al. (2016) was harvested at \sim 2 weeks (after 10 generations of acclimation), whereas our mesocosm was harvested at <1 week (no prior acclimation). Furthermore, a more complete proteome of P. nitzschia monoculture was measured for the 2016 laboratory study. In contrast, in this mesocosm study we had limited biomass (due to herbivory) and were sampled peptides from a diverse group within a $>5-\mu$ m subset of the community. Another unknown is whether genotype sorting could result on a timescale of days in the mesocosms (i.e., comparable to the time needed for one cell division cycle) particularly if selection pressure is strong (Collins et al. 2020). It was also difficult to assess the responses of longer-lived grazers (weeks to months) to these 2100 conditions, and, in the case of the heterotrophic bacteria, which exhibited pronounced increases in production in both mesocosms, we had insufficient metrics to diagnose the underlying reasons.

Wider extrapolation and links to model projections

Our findings on the future alteration of phytoplankton productivity are of the same sign as model projections for changes to regional NPP (Laufkötter et al. 2015; Kwiatkowski et al. 2020). The at least doubling of chlorophyll took place in the presence of a representative pelagic foodweb, and with heavy grazing pressure, suggesting that this cumulative outcome for phytoplankton under bottom-up (multiple drivers) and top-down control (subpolar foodweb) was conspicuous despite the high grazing rates, and points to the role of bottomup environmental control in shaping the outcome of this experiment (with the caveat of longer time scale of response to 2100 conditions for grazers). Although there were logistical issues, outlined above, associated with working with natural populations, in obtaining clear insights into the underpinning reasons for increased phytoplankton stocks, there is evidence of a decreased need for phosphate under warmer 2100 conditions that match reports from laboratory studies (Toseland et al. 2013; Boyd et al. 2016). There was also indirect evidence (see Table 2) from metaproteomics of the key role played by Fe supply (with lesser influences exerted by pH and irradiance) in the 2100 mesocosm. Hence, the underlying multiple (i.e., direct and indirect) roles of warming and increased Fe supply appear to be particularly influential during this mesocosm experiment. As introduced earlier, this suggests that manipulation studies exhibit, and models project, a more productive Southern Ocean, but that they are driven by a combination of different mechanisms. There are drawbacks to both approaches. Models within the CMIP6 model intercomparison face many ongoing challenges in representing the Fe cycle and the degree of phytoplankton Fe limitation in simulations (Séférian et al. 2020). There is also increasing evidence of subtle interactive effects on phytoplankton physiology driven by Fe and temperature (Andrew et al. 2019; Boyd 2019) that require incorporation into models. Laboratory and mesocosm experiments also face challenges since they employ batch culture methods resulting in transient effects. How applicable are these transient outcomes to seasonal scales?

Figure 8 summarizes different approaches used in laboratory and field manipulations and contrasts them with how models are used to generate future projections. Typically, Earth System Models use a single set of biological parameters,

some with temperature dependence. Given the climate forcing, the Earth System Model responds by determining the biology, chemistry and physics. Hence, nutrient supply (and nutrient drawdown) is an emergent behavior of the system, and not a property that can be directly controlled. So, in effect, such Earth System Models do not specifically differentiate between short-term and long-term responses, and thus it is difficult to compare directly with the "batch culture" approach used in Boyd et al. (2016) and our mesocosm study (Fig. 8). In the Earth System Model projections, the ecological imprint of climate change occurs gradually over many decades as a slow trend overlaying simulated internal variability on time-scales from episodic events (e.g., storms; dust deposition) to the seasonal cycle and interannual climate modes. The climate imprint in Fig. 8B (left panel) is represented, schematically, as a shift in the mean of a probability distribution function for an ocean variable, recognizing that the system will still contain substantial internal variability.

In principle, the batch culture approach used in perturbation experiments could be replicated in an ESM by adding a nutrient pulse, but this would only make sense if trying to mimic an atmospheric deposition event as opposed to changes in subsurface nutrient supply modulated by global ocean change and enhanced vertical stratification. Alternatively, laboratory cultures and mesocosms could be run in continuous mode, akin to a chemostat in which biological stocks are maintained in steady-state (at a pre-selected growth rate) by the supply of nutrients at the same rate as they are being washed out of the mesocosm (Fig. 8). While the future chemostat is represented in Fig. 8B (right panel) as a flat line, a slightly more realistic chemostat experiment could include variability in the nutrient supply that averages out to the same mean input flux similar to that exhibited by the future state in an Earth System Model. Such a chemostat-like approach would make them more comparable to model frameworks, extend their duration to explore longer-term grazer dynamics, and help to overcome the transient resource limitation effects observed in the present study. However, there would be difficulties in pursuing this approach, for example, the difficulty in removing actively swimming mesozooplankton via the chemostat "wash-out" as they tend to actively evade fluid flows (Santos et al. 2017). Mesozooplankton would likely accumulate in the mesocosms (Fig. 8) and hence there would no longer be a representative pelagic community within the incubation. Clearly, we need to improve the links between model and experimental designs if we are to be able to intercompare their projections and learnt from them. Ocean biogeochemical model skill is frequently evaluated for performance against observed geographical patterns, seasonal cycles, and interannual variability (Doney et al. 2009), but this does not guarantee, necessarily, skill in projecting responses to multidecadal climate change, particularly if slow processes are involved (e.g., evolutionary adaptation of plankton species). In the mesocosm experiments, on the other hand, the climate

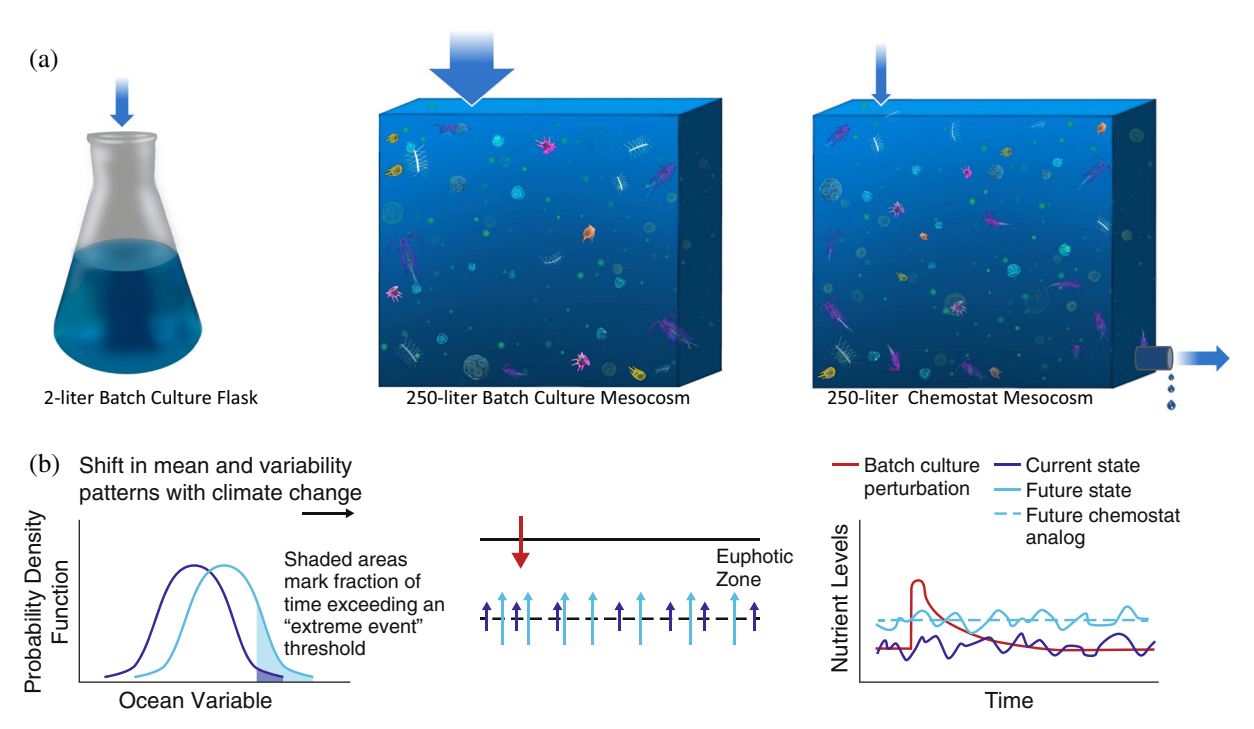


Fig. 8. Intercomparison of lab culture, shipboard mesocosms and numerical simulations used to mimic the effects of decade-scale ocean global change on marine life. From left to right in (A) presents the design of manipulation experiments used in the Boyd et al. (2016) lab culture study, mesocosms in the present study, and a hypothetical design of a flow-through chemostat mesocosm to avoid the transient effects observed in the present study. However, the latter will likely result in the retention of grazers such as mesozooplankton which actively avoid fluid flows (Santos et al. 2017). In panel (B) from left to right—the representation of ocean global change within numerical simulations, commencing with how climate change can alter the mean, width and shape of the distribution of a typical ocean variable; centre panel—examples for nutrient supply of how episodic atmospheric events are comparable to batch culture-like perturbation vs. the more continuous, chemostat-like perturbations of upwards nutrient supply from shifts in climate; right panel—mesocosm batch experiments follow the time response to transient perturbations that attempt to mimic shifts in mean state under climate change. Some perturbations can be maintained throughout the experiment (e.g., dashed line—temperature, CO₂) while others are transient (e.g., solid line—nutrient additions). Chemostats are also represented by the dashed line. Ocean model simulations reflect a mix of baseline shifts and variability.

change signal is compressed into an abrupt jump in the climate state, and the resulting rapid physiological acclimation and community shifts may also not capture longer-term responses. Both approaches have limitations and strengths that are complementary.

Conclusions

The resident phytoplankton community responded to projected year 2100 subantarctic conditions by doubling chlorophyll stocks despite heavy grazing pressure within a pelagic foodweb setting. There was indirect evidence of the role of temperature in reducing the phosphorus requirement of cells, and of the important role Fe plays on phytoplankton processes in this subantarctic region. These putative underpinning mechanisms differ subtly from those inferred from model simulations of the Southern Ocean.

There is evidence of three main trends from the metaproteomics dataset: (1) phytoplankton acclimation to altered conditions during the experiment, (2) species-specific temporal patterns in photosystem I and II, and (3) alternate strategies for Fe acquisition and complexation. In many cases, the level of detail from the metaproteomics far exceeded that for the physiological metrics, and thus omics were under-utilized in joint comparisons. These comparisons were also hindered by the transition to resource limitation that, based on physiological measurements, peaked on day 3, whereas most of the proteomic analysis revealed statistically significant changes at the end of the experiment on day 7. Better linkages of physiological metrics and omics are needed to better access the powerful diagnostics that they can jointly bring (Strzepek et al. 2022). There are also promising developments from the emergence of new phenomenological models based on simplistic geochemical/taxonomic principles that utilize a small fraction of the wealth of proteomics data (McCain et al. 2021).

The transition from laboratory to field studies provided a more realistic ecosystem setting, but resulted in a loss of the control associated with laboratory studies, resulting in (1) no "line-of-sight" into prior environmental history of cells, (2) in vitro acclimation (revealed by proteomics), (3) proteomic analysis of the mixed community (metaproteomics) rather than an individual species (proteomics), (4) a finite shipboard incubation timeframe, and (5) the need to employ some

unconventional manipulations (e.g., adding nutrients to the 'control' treatments). Clearly, more thought is needed to improve experimental designs that incorporate manipulation of multiple ocean properties and include foobwebs.

References

- Adly, C. L., J.-E. Tremblay, R. T. Powell, E. Armstrong, G. Peers, and N. M. Price. 2015. Response of heterotrophic bacteria in a mesoscale iron enrichment in the northeast subarctic Pacific Ocean. Limnol. Oceanogr. **60**: 136–148. doi:10.1002/lno.10013
- Alderkamp, A.-C., H. J. de Baar, R. J. Visser, and K. R. Arrigo. 2010. Can photoinhibition control phytoplankton abundance in deeply mixed water columns of the Southern Ocean? Limnol. Oceanogr. **55**: 1248–1264. doi:10.4319/lo. 2010.55.3.1248
- Alderkamp, A., and others. 2019. Effects of iron and light availability on phytoplankton photosynthetic properties in the Ross Sea. Mar. Ecol. Prog. Ser. 621: 33–50. doi:10.3354/ meps13000
- Andrew, S. M., H. T. Morell, R. F. Strzepek, P. W. Boyd, and M. J. Ellwood. 2019. Iron availability influences the tolerance of Southern Ocean phytoplankton to warming and elevated irradiance. Front. Mar. Sci. **6**: 681. doi:10.3389/fmars.2019.00681
- Banse, K., and D. English. 1997. Near-surface phytoplankton pigment from the coastal zone color scanner in the Subantarctic region southeast of New Zealand. Mar. Ecol. Prog. Ser. **156**: 51–66. doi:10.3354/meps156051
- Bindoff, N. L., and others. 2019. Changing ocean, marine ecosystems, and dependent communities, p. 477–587. *In* H.-O. Pörtner and others. [eds.], IPCC special report on the ocean and cryosphere in a changing climate, Cambridge University Press, UK.
- Bopp, L., and others. 2013. Multiple stressors of ocean ecosystems in the 21st century: Projections with CMIP5 models. Biogeosciences **10**: 6225–6245. doi:10.5194/bg-10-6225-2013
- Boyd, P. W., R. H. Goldblatt, and P. J. Harrison. 1999*a*. Mesozooplankton grazing manipulations during in vitro iron enrichment studies in the NE subarctic Pacific. Deep-Sea Res. (II Top. Stud. Oceanogr.) **46**: 2645–2668. doi:10. 1016/s0967-0645(99)00079-x
- Boyd, P. W., J. Laroche, M. Gall, R. Frew, and R. M. L. McKay. 1999b. Role of iron, light, and silicate in controlling algal biomass in subantarctic waters SE of New Zealand. J. Geophys. Res. Oceans **104**: 13395–13408. doi:10.1029/1999jc900009
- Boyd, P. W., and E. R. Abraham. 2001. Iron-mediated changes in phytoplankton photosynthetic competence during SOI-REE. Deep-Sea Res. (II Top. Stud. Oceanogr.) **48**: 2529. doi: 10.1016/s0967-0645(01)00007-8

- Boyd, P. W., and others. 2005. The evolution and termination of an iron-induced mesoscale bloom in the northeast subarctic Pacific. Limnol. Oceanogr. **50**: 1872–1886. doi:10. 4319/lo.2005.50.6.1872
- Boyd, P. W., and C. J. Brown. 2015. Modes of interactions between environmental drivers and marine biota. Front. Mar. Sci. 2: 9. doi:10.3389/fmars.2015.00009
- Boyd, P. W., S. T. Lennartz, D. M. Glover, and S. C. Doney. 2015. Biological ramifications of climate-change-mediated oceanic multi-stressors. Nat. Clim. Change **5**: 71–79. doi: 10.1038/nclimate2441
- Boyd, P. W., and others. 2016. Physiological responses of a Southern Ocean diatom to complex future ocean conditions. Nat. Clim. Change **6**: 207–213. doi:10.1038/nclimate2811
- Boyd, P. W., and others. 2018. Experimental strategies to assess the biological ramifications of multiple drivers of global ocean change a review. Glob. Chang. Biol. **24**: 2239–2261. doi:10.1111/gcb.14102
- Boyd, P. W. 2019. Physiology and iron modulate diverse responses of diatoms to a warming Southern Ocean. Nat. Clim. Change **9**: 148–152. doi:10.1038/s41558-018-0389-1
- Bradford-Grieve, J., R. Murdoch, M. James, M. Oliver, and J. McLeod. 1998. Mesozooplankton biomass, composition, and potential grazing pressure on phytoplankton during austral winter and spring 1993 in the subtropical convergence region near New Zealand. Deep-Sea Res. (I Oceanogr. Res. Pap.) **45**: 1709–1737. doi:10.1016/S0967-0637(98) 00039-9
- Brennan, G., and S. Collins. 2015. Growth responses of a green alga to multiple environmental drivers. Nat. Clim. Change **5**: 892–897. doi:10.1038/nclimate2682
- Chown, S. L. 2020. Marine food webs destabilized. Science **369**: 770–771. doi:10.1126/science.abd5739
- Church, M. J., D. A. Hutchins, and H. W. Ducklow. 2000. Limitation of bacterial growth by dissolved organic matter and iron in the Southern Ocean. Appl. Environ. Microbiol. **66**: 455–466. doi:10.1128/AEM.66.2.455-466.2000
- Coale, T. H., M. Moosburner, A. Horák, M. Oborník, K. A. Barbeau, and A. E. Allen. 2019. Reduction-dependent siderophore assimilation in a model pennate diatom. Proc. Natl. Acad. Sci. 116: 23609. doi:10.1073/pnas.1907234116
- Collins, S., P. W. Boyd, and M. A. Doblin. 2020. Evolution, microbes, and changing ocean conditions. Ann. Rev. Mar. Sci. **12**: 181–208. doi:10.1146/annurev-marine-010318-095311
- Denman, K., and A. Gargett. 1983. Time and space scales of vertical mixing and advection of phytoplankton in the upper ocean. Limnol. Oceanogr. **28**: 801–815. doi:10.4319/lo.1983.28.5.0801
- Deppeler, S. L., and A. T. Davidson. 2017. Southern Ocean phytoplankton in a changing climate. Front. Mar. Sci. **4**: 40. doi:10.3389/fmars.2017.00040
- Deutsch, E. W., and others. 2019. The ProteomeXchange consortium in 2020: Enabling 'big data' approaches in

- proteomics. Nucleic Acids Res. **48**: D1145–D1152. doi:10. 1093/nar/gkz984
- Doney, S. C., and others. 2009. Skill metrics for confronting global upper ocean ecosystem-biogeochemistry models against field and remote sensing data. J. Mar. Syst. **76**: 95–112. doi:10.1016/j.jmarsys.2008.05.015
- Doney, S. C. 2010. The growing human footprint on coastal and Open-Ocean biogeochemistry. Science **328**: 1512–1516. doi:10.1126/science.1185198
- Ellwood, M. J., and others. 2015. Iron stable isotopes track pelagic iron cycling during a subtropical phytoplankton bloom. Proc. Natl. Acad. Sci. **112**: E15–E20. doi:10.1073/pnas.1421576112
- Ellwood, M. J., R. F. Strzepek, P. G. Strutton, T. W. Trull, M. Fourquez, and P. W. Boyd. 2020. Distinct iron cycling in a Southern Ocean eddy. Nat. Commun. **11**: 825. doi:10. 1038/s41467-020-14464-0
- Eriksen, R., T. W. Trull, D. Davies, P. Jansen, A. T. Davidson, K. Westwood, and R. van den Enden. 2018. Seasonal succession of phytoplankton community structure from autonomous sampling at the Australian Southern Ocean Time Series (SOTS) observatory. Mar. Ecol. Prog. Ser. **589**: 13–31. doi:10.3354/meps12420
- Fourquez, M., M. Bressac, S. L. Deppeler, M. Ellwood, I. Obernosterer, T. W. Trull, and P. W. Boyd. 2020. Microbial competition in the subpolar Southern Ocean: An Fe–C Colimitation experiment. Front. Mar. Sci. **6**: 776. doi:10.3389/fmars.2019.00776
- Goldblatt, R. H., D. L. Mackas, and A. G. Lewis. 1999. Mesozooplankton community characteristics in the NE subarctic Pacific. Deep-Sea Res. (II Top. Stud. Oceanogr.) **46**: 2619. doi:10.1016/s0967-0645(99)00078-8
- Harris, G. P., F. B. Griffiths, and D. P. Thomas. 1989. Light and dark uptake and loss of ¹⁴C: Methodological problems with productivity measurements in oceanic waters. Hydrobiologia **173**: 95–105. doi:10.1007/BF00015519
- Hoppe, C. J. M., C. S. Hassler, C. D. Payne CD, P. D. Tortell, B. Rost, and S. Trimborn. 2013. Iron limitation modulates ocean acidification effects on Southern Ocean phytoplankton communities. PLoS One 8: e79890. doi:10.1371/journal.pone.0079890
- Hoppe, C. J. M., N. Schuback, D. M. Semeniuk, M. T. Maldonado, and B. Rost. 2017. Functional redundancy facilitates resilience of subarctic phytoplankton assemblages toward ocean acidification and high irradiance. Front. Mar. Sci. 4: 229. doi:10.3389/fmars.2017.00229
- Hudson, R. J. M., D. T. Covault, and F. M. M. Morel. 1992. Investigations of iron coordination and redox reactions in seawater using 59Fe radiometry and ion-pair solvent extraction of amphiphilic iron complexes. Mar. Chem. **38**: 209–235. doi:10.1016/0304-4203(92)90035-9
- Jabre, L., and E. M. Bertrand. 2020. Interactive effects of iron and temperature on the growth of Fragilariopsis cylindrus.

- Limnol. Oceanogr. Lett. **5**: 363–370. doi:10.1002/lol2. 10158
- Jabre, L. J., and others. 2021. Molecular underpinnings and biogeochemical consequences of enhanced diatom growth in a warming Southern Ocean. Proc. Natl. Acad. Sci. **118**: e2107238118. doi:10.1073/pnas.2107238118
- Kwiatkowski, L., O. Aumont, L. Bopp, and P. Ciais. 2018. The impact of variable phytoplankton stoichiometry on projections of primary production, food quality, and carbon uptake in the Global Ocean. Global Biogeochem. Cycles **32**: 516–528. doi:10.1002/2017GB005799
- Kwiatkowski, L., and others. 2020. Twenty-first century ocean warming, acidification, deoxygenation, and upper-ocean nutrient and primary production decline from CMIP6 model projections. Biogeosciences **17**: 3439–3470. doi:10. 5194/bg-17-3439-2020
- Laufkötter, C., and others. 2015. Drivers and uncertainties of future global marine primary production in marine ecosystem models. Biogeosciences **12**: 6955–6984. doi:10.5194/bg-12-6955-2015
- Li, W. K. W. 1982. Estimating heterotrophic bacterial productivity by inorganic radiocarbon uptake: Importance of establishing time courses of uptake. Mar. Ecol. Prog. Ser. 8: 167–172.
- Lis, H., Y. Shaked, C. Kranzler, N. Keren, and F. M. M. Morel. 2015. Iron bioavailability to phytoplankton: An empirical approach. ISME J. **9**: 1003–1013. doi:10.1038/ismej. 2014.199
- Liu, X., M. C. Patsavas, and R. H. Byrne. 2011. Purification and characterization of meta-cresol purple for spectrophotometric seawater pH measurements. Environ. Sci. Technol. **45**: 4862–4868. doi:10.1021/es200665d
- Lyon, B. R., and T. Mock. 2014. Polar microalgae: New approaches towards understanding adaptations to an extreme and changing environment. Biology **3**: 56–80. doi: 10.3390/biology3010056
- McCain, J. S. P., A. Tagliabue, E. Susko, E. P. Achterberg, A. E. Allen, and E. M. Bertrand. 2021. Cellular costs underpin micronutrient limitation in phytoplankton. Sci. Adv. **7**: 6501. doi:10.1126/sciadv.abg6501
- Meyerink, S. W., P. W. Boyd, W. A. Maher, A. Milne, R. Strzepek, and M. J. Ellwood. 2019. Putting the silicon cycle in a bag: Field and mesocosm observations of silicon isotope fractionation in subtropical waters east of New Zealand. Mar. Chem. **213**: 1–12. doi:10.1016/j. marchem.2019.04.008
- Mikan, M. P., and others. 2020. Metaproteomics reveal that rapid perturbations in organic matter prioritize functional restructuring over taxonomy in western Arctic Ocean microbiomes. ISME J. **14**: 39–52. doi:10.1038/s41396-019-0503-z
- Moreau, S., P. W. Boyd, and P. G. Strutton. 2020. Remote assessment of the fate of phytoplankton in the Southern

- Ocean sea-ice zone. Nat. Commun. **11**: 3108. doi:10.1038/s41467-020-16931-0
- Moreno, C. M., Y. Lin, S. Davies, E. Monbureau, N. Cassar, and A. Marchetti. 2018. Examination of gene repertoires and physiological responses to iron and light limitation in Southern Ocean diatoms. Polar Biol. **41**: 679–696. doi:10. 1007/s00300-017-2228-7
- Moreno, C. M., W. Gong, N. R. Cohen, K. DeLong, and A. Marchetti. 2020. Interactive effects of iron and light limitation on the molecular physiology of the Southern Ocean diatom Fragilariopsis kerguelensis. Limnol. Oceanogr. **65**: 1511–1531. doi:10.1002/lno.11404
- Nagelkerken, I., S. U. Goldenberg, C. M. Ferreira, H. Ullah, and S. D. Connell. 2020. Trophic pyramids reorganize when food web architecture fails to adjust to ocean change. Science **369**: 829–832. doi:10.1126/science.aax0621
- Nunn, B., and others. 2009. Deciphering diatom biochemical pathways via whole-cell proteomics. Aquat. Microb. Ecol. **55**: 241–253. doi:10.3354/ame01284
- Nunn, B. L., and others. 2013. Diatom proteomics reveals unique acclimation strategies to mitigate Fe limitation. PLoS One **8**: e75653. doi:10.1371/journal.pone.0075653
- Parkhill, J.-P., G. Maillet, and J. J. Cullen. 2001. Fluorescence-based maximal quantum yield for PSII as a diagnostic of nutrient stress. J. Phycol. **37**: 517–529. doi:10.1046/j.1529-8817.2001.037004517.x
- Perez-Riverol, Y., and others. 2019. The PRIDE database and related tools and resources in 2019: Improving support for quantification data. Nucleic Acids Res. **47**: D442–D450. doi:10.1093/nar/gky1106
- Petrou, K., and others. 2016. Southern Ocean phytoplankton physiology in a changing climate. J. Plant Physiol. **203**: 135–150. doi:10.1016/j.jplph.2016.05.004
- Pörtner, H.-O., and others. 2014. Ocean systems, p. 411–484. *In* Climate change 2014: Impacts, adaptation, and vulnerability. Part a: Global and sectoral aspects. Contribution of working group II to the fifth assessment report of the intergovernmental panel on climate change. Cambridge Univ. Press.
- Quero, G. M., M. Celussi, F. Relitti, V. Kovačević, P. Del Negro, and G. M. Luna. 2020. Inorganic and organic carbon uptake processes and their connection to microbial diversity in Meso- and bathypelagic Arctic waters (eastern Fram Strait). Microb. Ecol. **79**: 823–839. doi:10.1007/s00248-019-01451-2
- R Core Team (2013). R: A language and environment for statistical computing. R Foundation for Statistical Computing. http://www.R-project.org/.
- Raven, J. A., and F. A. Smith. 1974. Significance of hydrogen ion transport in plant cells. Can. J. Bot. **52**: 1035–1048.
- Riebesell, U., and others. 2018. Toxic algal bloom induced by ocean acidification disrupts the pelagic food web. Nat. Clim. Change **8**: 1082–1086. doi:10.1038/s41558-018-0344-1
- Riffle, M., D. H. May, E. Timmins-Schiffman, M. P. Mikan, D. Jaschob, W. S. Noble, and B. L. Nunn. 2018. MetaGOmics:

- A web-based tool for peptide-centric functional and taxonomic analysis of Metaproteomics data. Proteomes **6**: 2. doi:10.3390/proteomes6010002
- Santos, G. S., M. Brito-Lolaia, and R. Schwamborn. 2017. Two new methods for sampling zooplankton and larval assemblages in tropical reef ecosystems. J. Exp. Mar. Biol. Ecol. **491**: 27–37. doi:10.1016/j.jembe.2017.03.008
- Schulz, E. W., S. A. Josey, and R. Verein. 2012. First air-sea flux mooring measurements in the Southern Ocean. Geophys. Res. Lett. **39**: 52290. doi:10.1029/2012GL052290
- Séférian, R., and others. 2020. Tracking improvement in simulated marine biogeochemistry between CMIP5 and CMIP6. Curr. Clim. Chang. Rep. **6**: 95–119. doi:10.1007/s40641-020-00160-0
- Shadwick, E. H., T. W. Trull, B. Tilbrook, A. J. Sutton, E. Schulz, and C. L. Sabine. 2015. Seasonality of biological and physical controls on surface ocean CO₂ from hourly observations at the Southern Ocean Time Series site south of Australia. Global Biogeochem. Cycles **29**: 223–238. doi: 10.1002/2014GB004906
- Shi, D., Y. Xu, B. M. Hopkinson, and F. M. M. Morel. 2010. Effect of ocean acidification on iron availability to marine phytoplankton. Science **327**: 676–679. doi:10.1126/science.1183517
- Sommer, U., and K. Lengfellner. 2008. Climate change and the timing, magnitude, and composition of the phytoplankton spring bloom. Glob. Chan. Biol. **14**: 1199–1208. doi:10.1111/j.1365-2486.2008.01571.x
- Steinberg, D. K., and M. R. Landry. 2017. Zooplankton and the ocean carbon cycle. Ann. Rev. Mar. Sci. **9**: 413–444. doi:10.1146/annurev-marine-010814-015924
- Strzepek, R. F., M. T. Maldonado, J. L. Higgins, J. Hall, K. Safi, S. W. Wilhelm, and P. W. Boyd. 2005. Spinning the "Ferrous Wheel": The importance of the microbial community in an iron budget during the FeCycle experiment. Global Biogeochem. Cycles **19**: 2490. doi:10.1029/2005GB002490
- Strzepek, R. F., K. A. Hunter, R. D. Frew, P. J. Harrison, and P. W. Boyd. 2012. Iron-light interactions differ in Southern Ocean phytoplankton. Limnol. Oceanogr. **57**: 1182–1200. doi:10.4319/lo.2012.57.4.1182
- Strzepek, R. F., P. W. Boyd, and W. G. Sunda. 2019. Photosynthetic adaptation to low iron, light, and temperature in Southern Ocean phytoplankton. Proc. Natl. Acad. Sci. **116**: 4388. doi:10.1073/pnas.1810886116
- Strzepek, R. F., B. L. Nunn, L. T. Bach, J. A. Berges, E. B. Young, and P. W. Boyd. 2022. The ongoing need for rates: can physiology and omics come together to co-design the measurements needed to understand complex ocean biogeochemistry?. J. Plankton Res. (2022) 1–11. doi:10.1093/plankt/fbac026
- Suggett, D., C. Moore, A. Hickman, and R. Geider. 2009. Interpretation of fast repetition rate (FRR) fluorescence: Signatures of phytoplankton community structure versus physiological state. Mar. Ecol. Prog. Ser. **376**: 1–19. doi:10. 3354/meps07830

- Sunda, W., and S. Huntsman. 2003. Effect of pH, light, and temperature on Fe–EDTA chelation and Fe hydrolysis in seawater. Mar. Chem. **84**: 35–47. doi:10.1016/S0304-4203(03)00101-4
- Sunda, W. G., and S. A. Huntsman. 2011. Interactive effects of light and temperature on iron limitation in a marine diatom: Implications for marine productivity and carbon cycling. Limnol. Oceanogr. **56**: 1475–1488. doi:10.4319/lo. 2011.56.4.1475
- Takeda, S. 1998. Influence of iron availability on nutrient consumption ratio of diatoms in oceanic waters. Nature **393**: 774–777. doi:10.1038/31674
- Taylor, A. R., A. Chrachri, C. Wheeler, H. Goddard, and C. Brownlee. 2011. A voltage-gated H+ channel underlies pH homeostasis in calcifying coccolithophores. PLoS Biology **9**: art. e1001085.
- Timmermans, K. R., B. Van Der Wagt, and H. J. W. de Baar. 2004. Growth rates, half saturation constants, and silicate, nitrate, and phosphate depletion in relation to iron availability of four large open-ocean diatoms from the Southern Ocean. Limnol. Oceanogr. **49**: 2141–2151. doi:10.4319/lo. 2004.49.6.2141
- Toei, M., R. Saum, and M. Forgac. 2010. Regulation and isoform function of the V-ATPases. Biochemistry **49**: 4715–4723. doi:10.1021/bi100397s, PMID: 20450191
- Toseland, A., and others. 2013. The impact of temperature on marine phytoplankton resource allocation and metabolism. Nat. Clim. Change **3**: 979–984. doi:10.1038/nclimate1989
- Trimborn, S., T. Brenneis, C. J. M. Hoppe, L. M. Laglera, and others. 2017. Iron sources alter the response of Southern Ocean phytoplankton to ocean acidification. Mar. Ecol. Prog. Ser. **578**: 35–50. doi:10.3354/meps12250
- Weeding, B., and T. W. Trull. 2014. Hourly oxygen and total gas tension measurements at the Southern Ocean Time

- Series site reveal winter ventilation and spring net community production. J. Geophys. Res. Oceans **119**: 348–358. doi:10.1002/2013JC009302
- Wu, M., J. S. P. McCain, E. Rowland, R. Middag, M. Sandgren, A. E. Allen, and E. M. Bertrand. 2019. Manganese and iron deficiency in Southern Ocean Phaeocystis Antarctica populations revealed through taxon-specific protein indicators. Nat. Commun. 10: 3582. doi:10.1038/s41467-019-11426-z

Acknowledgments

The ship time for this research was financially supported by Australia's Marine National Facility. The authors are grateful to the officers, crew, and research staff of the Marine National Facility and the R.V. Investigator for their help with sample collection and generation of hydrochemistry data. The authors thank Tasman Nunn for her illustrations in Fig. 8. MJE, RS, and PWB were financially supported under Australian Research Council's Discovery program (DP170102108; DP130100679). SCD acknowledges support from the U.S. National Science Foundation (PLR-2026045). This research was financially supported under Australian Research Council's Discovery program (DP170102108; DP130100679). BLN and ETS were funded by the National Science Foundation (IOS-2041497 and OCE-1633939) and the proteomics work was partially supported by the University of Washington Proteomics Resource Grant (UWPR95794). Open access publishing facilitated by University of Tasmania, as part of the Wiley - University of Tasmania agreement via the Council of Australian University Librarians.

Conflict of interest

None declared

Submitted 15 September 2021 Revised 20 February 2022 Accepted 28 May 2022

Deputy editor: C. Elisa Schaum